

CERN-EP-2018-141
2019/03/05

CMS-HIG-16-042

Measurements of properties of the Higgs boson decaying to a W boson pair in pp collisions at $\sqrt{s} = 13$ TeV

The CMS Collaboration*

Abstract

Measurements of the production of the standard model Higgs boson decaying to a W boson pair are reported. The W^+W^- candidates are selected in events with an oppositely charged lepton pair, large missing transverse momentum, and various numbers of jets. To select Higgs bosons produced via vector boson fusion and associated production with a W or Z boson, events with two jets or three or four leptons are also selected. The event sample corresponds to an integrated luminosity of 35.9 fb^{-1} , collected in pp collisions at $\sqrt{s} = 13$ TeV by the CMS detector at the LHC during 2016. Combining all channels, the observed cross section times branching fraction is $1.28_{-0.17}^{+0.18}$ times the standard model prediction for the Higgs boson with a mass of 125.09 GeV. This is the first observation of the Higgs boson decay to W boson pairs by the CMS experiment.

Published in Physics Letters B as doi:10.1016/j.physletb.2018.12.073.

1 Introduction

In the standard model (SM) of particle physics, the origin of the masses of the W and Z bosons is based on the spontaneous breaking of the electroweak symmetry. This symmetry breaking is achieved through the introduction of a complex doublet scalar field [1–6], leading to the prediction of the existence of one physical neutral scalar particle, commonly known as the Higgs boson (H). The observation of a new particle at a mass of approximately 125 GeV with Higgs boson-like properties was reported by the ATLAS [7] and CMS [8, 9] Collaborations during the first running period of the CERN LHC in proton-proton (pp) collisions at center-of-mass energies of 7 and 8 TeV. Subsequent publications from both collaborations, based on the 7 and 8 TeV data sets [10–13], established that all measured properties of the new particle, including its spin, parity, and coupling strengths to SM particles, are consistent within the uncertainties with those expected for the SM Higgs boson. A combination of the ATLAS and CMS results [14, 15] further confirmed these observations and resulted in determining the boson mass to be $m_H = 125.09 \pm 0.21$ (stat) ± 0.11 (syst) GeV.

The Higgs boson decay to a pair of W bosons was studied by the ATLAS and CMS Collaborations using the 7 and 8 TeV data sets in leptonic final states, exploring several production mechanisms [16–18]. The probability of observing a signal at least as large as the one seen, under the background-only hypothesis, corresponded to a significance of 6.5 and 4.3 standard deviations (s.d.) for ATLAS and CMS respectively, while the expected significance for a SM Higgs boson was 5.8 (5.9) s.d. for the CMS (ATLAS) collaboration. A later CMS combination [12], that includes Higgs boson production in association with a top quark pair, reported an observed significance of 4.7 s.d. for this decay. The same decay channel was used by the ATLAS and CMS Collaborations to search for the Higgs boson off-shell production [19, 20] and to perform fiducial and differential cross section measurements [21, 22].

In 2015, the LHC restarted at $\sqrt{s} = 13$ TeV, delivering high luminosity pp collisions. The new data are used to further constrain the properties of the Higgs boson: any significant deviation from the SM predictions would be a clear sign of new physics. This paper presents the analysis of the $H \rightarrow WW$ decay at 13 TeV, using a data sample corresponding to a total integrated luminosity of 35.9 fb^{-1} , collected during 2016. The same final state was recently studied by ATLAS [23] using 2015 and 2016 data.

Gluon fusion (ggH) is the dominant production mode for a Higgs boson with a mass of 125 GeV in pp collisions at $\sqrt{s} = 13$ TeV. The large Higgs boson branching fraction to a W boson pair makes this channel suitable for a precision measurement of the Higgs boson production cross section, and also allows studies of subleading production channels, such as Higgs boson production via vector boson fusion (VBF) and associated production with a vector boson (VH). These channels are also studied in this paper, contributing to the precision in the measurement of the Higgs boson couplings.

The leptonic decays of the two W bosons provide the cleanest decay channel, despite the presence of neutrinos in the final state that prevents the full reconstruction of the Higgs boson mass. The different-flavor (DF) leptonic decay mode $e\mu$ has the largest branching fraction, is the least affected by background processes, and therefore is the most sensitive channel of the analysis. The same-flavor (SF) e^+e^- and $\mu^+\mu^-$ final states are also considered, although their sensitivity is limited by the contamination from the Drell–Yan (DY) background with missing transverse momentum due to instrumental effects.

Events with a pair of oppositely charged leptons (electrons and/or muons) and missing transverse momentum, due to the presence of neutrinos in the final state, are selected. This signa-

ture is common to other SM processes that contribute to the background in this analysis. The main contribution comes from nonresonant production of W boson pairs (WW), an irreducible background that shares the same final state and can only be separated from the signal using kinematic distributions. Backgrounds coming from top quark events ($t\bar{t}$ and tW) are also important, followed by other processes, such as W +jets and other diboson and triboson production processes. The DY process is the dominant source of background in the dielectron and dimuon final states, while it is subdominant in the electron-muon final state, since its contribution arises from the leptonic decays of the τ leptons emerging from $Z/\gamma^* \rightarrow \tau^+\tau^-$.

The events are categorized by jet multiplicity to better handle the $t\bar{t}$ background. In addition, dedicated categories are designed to enhance the sensitivity to the VBF and VH production mechanisms.

2 The CMS detector

The CMS detector is a multipurpose apparatus designed to study high transverse momentum (p_T) physics processes in proton-proton and heavy ion collisions, and is described in detail in Ref. [24] together with a definition of the coordinate system used. A superconducting solenoid occupies its central region, providing a magnetic field of 3.8 T parallel to the beam direction. Charged particle trajectories are measured by the silicon pixel and strip trackers, which cover a pseudorapidity region of $|\eta| < 2.5$. A lead tungstate crystal electromagnetic calorimeter (ECAL), and a brass and scintillator hadron calorimeter surround the tracking volume and cover $|\eta| < 3$. The steel and quartz fiber Cherenkov hadron forward calorimeter extends the coverage to $|\eta| < 5$. The muon system consists of gas-ionization detectors embedded in the steel flux-return yoke outside the solenoid, and covers $|\eta| < 2.4$. The first level of the CMS trigger system, composed of custom hardware processors, is designed to select the most interesting events in less than $4 \mu\text{s}$, using information from the calorimeters and muon detectors. The high-level trigger processor farm further reduces the event rate to about 1000 Hz, before data storage.

3 Data and simulated samples

The events used in this analysis are selected by high-level trigger algorithms that require the presence of one or two high- p_T electrons or muons passing loose identification and isolation requirements. In single-lepton triggers, relatively tight lepton identification criteria are applied. The p_T threshold is 25 GeV in the central region ($|\eta| < 2.1$) and 27 GeV for $2.1 < |\eta| < 2.5$ for electrons, while it is 24 GeV for muons ($|\eta| < 2.4$). In the dielectron trigger, the minimum required p_T is 23 GeV for the leading and 12 GeV for the subleading electron. In the dimuon trigger, the minimum p_T is 17 GeV for the leading and 8 GeV for the subleading muon. In the two dilepton $e\mu$ triggers used in the analysis, the minimum p_T requirements are either 8 GeV for the muon and 23 GeV for the electron, or 23 GeV for the muon and 12 GeV for the electron. The combination of single-lepton and dilepton triggers provides an overall trigger efficiency in excess of 98% for selected signal events.

Several event generators are used to optimize the analysis and estimate the expected yields of signal and backgrounds, as well as their associated systematic uncertainties. Different Higgs boson production mechanisms are simulated. Both ggH and VBF are generated with POWHEG v2 [25–28], which describes the full next-to-leading order (NLO) perturbative quantum chromodynamics (QCD) properties of these processes. In addition, the ggH process is reweighted to match the Higgs boson p_T and the number of associated jets to the prediction of POWHEG

NNLOPS [29], which provides a next-to-next-to-leading order (NNLO) description for the inclusive Higgs boson production, NLO for the exclusive $H + 1$ jet production, and leading order (LO) for the exclusive $H + 2$ jets production. The reweighting is performed by computing the ratio of the Higgs boson p_T distribution from the NNLOPS generator to that from the POWHEG generator in each jet multiplicity bin, and applying this ratio to the ggH POWHEG simulation. The MINLO HVJ [30] extension of POWHEG is used to simulate the associated production of the Higgs boson with vector bosons (W^+H , W^-H , ZH), which simulates the $VH + 0$ and 1 jet processes with NLO accuracy. Higgs boson production in association with top or bottom quarks, such as $t\bar{t}H$ and $b\bar{b}H$ production mechanisms, are considered as well, although they only contribute to a minor extent in the phase space selected by this analysis. For the simulation of $t\bar{t}H$ production the POWHEG generator is used, while the MADGRAPH5_aMC@NLO v2.2.2 generator [31] is used to simulate the $b\bar{b}H$ production. The Higgs boson is generated with a mass of 125.09 GeV and is made to decay into a pair of W bosons, considering only leptonic W boson decays (e , μ , or τ). For Higgs bosons produced via ggH [32] and VBF [33] processes, their decay into two W bosons and subsequently into leptons is simulated using JHUGEN v5.2.5 [34, 35]. For the associated production mechanisms, including gluon fusion produced ZH, the Higgs boson decay and the associated vector boson inclusive decays are simulated by PYTHIA 8.212 [36]. The simulated signal samples are normalized using cross sections [37] and decay rates [38] computed by the LHC Higgs Cross Section Working Group. In particular the most recent next-to-next-to-next-to-leading order calculations for the inclusive gluon fusion production are used [37]. Additional simulated samples, where the Higgs boson decays into a pair of τ leptons, are also produced for each of the aforementioned production mechanisms. Unless stated otherwise, the $H \rightarrow \tau\tau$ events passing the selection are considered signal events in the signal yield determination. However, their expected contribution in the signal phase space is small compared to $H \rightarrow W^+W^-$.

The various background processes in this study are simulated as follows: POWHEG v2 [39] is used for $q\bar{q} \rightarrow WW$ production, whereas $gg \rightarrow WW$ production is generated using MCFM v7.0 [40]. A WW simulation with two additional jets is generated with MADGRAPH5_aMC@NLO at LO accuracy via diagrams with six electroweak (EW) vertices, referred to as WW EW production. In order to suppress the top quark background processes, the analysis is performed defining event categories with different number of high- p_T jets ($p_T > 30$ GeV). The classification of the events in bins of jet multiplicity spoils the convergence of fixed-order calculations of the $q\bar{q} \rightarrow WW$ process and requires the use of dedicated resummation techniques for an accurate prediction of the differential distributions [41, 42]. The simulated $q\bar{q} \rightarrow WW$ events are therefore reweighted to reproduce the p_T^{WW} distribution from the p_T -resummed calculation.

The LO cross section for the $gg \rightarrow WW$ process is obtained directly from MCFM. For this process, the difference between LO and NLO cross sections is significant; a K factor of 1.4 is calculated [43] and applied to the $gg \rightarrow WW$ simulation. Given the theoretical uncertainties in the K factor, and that it is mildly sensitive to the invariant mass of the WW system (m_{WW}) in the phase space of interest, an m_{WW} -independent calculation is used.

Single top quark and $t\bar{t}$ processes are generated using POWHEG v2. The cross sections of the different single top quark processes are estimated at NLO accuracy [44], while the $t\bar{t}$ cross section is computed at NNLO accuracy, with next-to-next-to-leading-logarithmic soft-gluon resummation [45].

The DY production of Z/γ^* is generated using MADGRAPH5_aMC@NLO at NLO accuracy using the FxFx jet matching and merging scheme with a merging scale $\mu_Q = 30$ GeV [46], and the Z/γ^* p_T distribution reweighted to match the distribution observed in data in dimuon events.

The $W\gamma^*$ background was simulated with POWHEG at NLO accuracy, down to a minimum invariant mass of the virtual photon of 100 MeV. The effect of the γ^* mass cutoff was estimated with a MADGRAPH5_aMC@NLO $W\gamma$ LO sample, in which the photon pair production was simulated by PYTHIA in the parton shower approximation. The impact from events in which the γ^* mass is below 100 MeV was found to be one order of magnitude smaller than the uncertainties quoted in this analysis, thus their contribution was neglected.

Other multiboson processes, such as WZ, ZZ, and VVV ($V = W, Z$), are also simulated with MADGRAPH5_aMC@NLO at NLO accuracy.

All processes are generated using the NNPDF 3.0 [47, 48] parton distribution functions (PDFs), with the accuracy matching that of the matrix element calculations. All the event generators are interfaced to PYTHIA for the showering of partons and hadronization, as well as the simulation of the underlying event (UE) and multiple-parton interactions based on the CUET8PM1 tune [49].

To estimate the systematic uncertainties related to the choice of the UE and multiple-parton interactions tune, the signal processes and the WW background are also generated with alternative tunes, which are representative of the uncertainties in the CUET8PM1 tuning parameters. The systematic uncertainty associated with showering and hadronization is estimated by interfacing the same samples with the HERWIG++ 2.7 generator [50, 51], using the UE-EE-5C tune for the simulation of UE and multiple-parton interactions [49].

For all processes, the detector response is simulated using a detailed description of the CMS detector, based on the GEANT4 package [52]. Additional simulated minimum bias pp interactions from PYTHIA are overlapped with the event of interest in each collision to reproduce the number of interactions per bunch crossing (pileup) measured in data. The average number of pileup interactions is about 27 per event for the 2016 data set used in this analysis.

4 Analysis strategy

A particle-flow (PF) algorithm [53] is used to reconstruct the observable particles in the event. Energy deposits (clusters) measured by the calorimeters and charged particle tracks identified in the central tracking system and the muon detectors are combined to reconstruct individual particles.

Among the vertices reconstructed in the event, the one with the largest value of summed physics-object p_T^2 is taken to be the primary pp interaction vertex. The physics objects include those returned by a jet-finding algorithm [54, 55] applied to all charged tracks assigned to the vertex, and the associated missing transverse momentum, defined as the negative vector sum of the p_T of those objects.

Electrons are reconstructed by matching clusters in the ECAL to tracks in the silicon tracker [56]. In this analysis, electron candidates are required to have $|\eta| < 2.5$. Additional requirements are applied to reject electrons originating from photon conversions in the tracker material or jets misreconstructed as electrons. Electron identification criteria rely on observables sensitive to the bremsstrahlung along the electron trajectory, the geometrical and momentum-energy matching between the electron track and the associated energy cluster in the ECAL, as well as ECAL shower shape observables and association with the primary vertex.

Muon candidates are reconstructed in the geometrical acceptance $|\eta| < 2.4$ by combining information from the silicon tracker and the muon system. Identification criteria based on the

number of measurements in the tracker and in the muon system, the fit quality of the muon track, and its consistency with its origin from the primary vertex are imposed on the muon candidates to reduce the misidentification rate.

Prompt leptons coming from EW interactions are usually isolated, whereas misidentified leptons and leptons coming from jets are often accompanied by charged or neutral particles, and can arise from a secondary vertex. Hence charged leptons are required to satisfy the isolation criterion that the p_T sum over charged PF candidates associated with the primary vertex, exclusive of the lepton itself, and neutral PF particles in a cone of a radius $\Delta R = \sqrt{(\Delta\phi)^2 + (\Delta\eta)^2} = 0.4$ (0.3), where ϕ is the azimuthal angle in radians, centered on the muon (electron) direction is below a threshold of 15 (6)% relative to the muon (electron) p_T . To mitigate the effect of the pileup on this isolation variable, a correction based on the average energy density in the event [57] is applied. Additional requirements on the transverse ($|d_{xy}|$) and longitudinal ($|d_z|$) impact parameters with respect to the primary vertex are included. Electrons detected by the ECAL barrel are required to have $|d_z| < 0.10$ cm and $|d_{xy}| < 0.05$ cm, while electrons in the ECAL endcap must satisfy $|d_z| < 0.20$ cm and $|d_{xy}| < 0.10$ cm. For muons, the $|d_z|$ parameter is required to be less than 0.10 cm, while $|d_{xy}|$ is required to be less than 0.01 cm for muons with $p_T < 20$ GeV and less than 0.02 cm for $p_T > 20$ GeV.

The jet reconstruction starts with all PF candidates, and removes the charged ones that are not associated with the primary vertex to mitigate the pileup impact. The remaining charged PF candidates and all neutral candidates are clustered by the anti- k_T algorithm [54] with a distance parameter of 0.4. To reduce further the residual pileup contamination from neutral PF candidates, a correction based on the jet area [57] is applied. The jet energy is calibrated using both simulation and data following the technique described in Ref. [58]. To identify jets coming from b quarks (b jets), a multivariate (MVA) b tagging algorithm is used [59]. In this analysis, the chosen working point corresponds to about 80% efficiency for genuine b jets, and to a mistagging rate of about 10% for light-quark or gluon jets and of 35 to 50% for c jets. A per-jet scale factor is computed and applied to account for b tagging efficiency and mistagging rate differences between data and simulation.

The missing transverse momentum vector (\vec{p}_T^{miss}), whose magnitude is denoted as p_T^{miss} , is reconstructed as the negative vectorial sum in the transverse plane of all PF particle candidate momenta. Since the presence of pileup induces a degradation of the p_T^{miss} measurement, affecting mostly backgrounds with no genuine p_T^{miss} , such as DY production, another p_T^{miss} that is constructed from only the charged particles (track p_T^{miss}) is used in events with an SF lepton pair (ee or $\mu\mu$). To suppress the remaining off-peak DY contribution in categories containing events with an SF lepton pair, a dedicated MVA selection based on a boosted decision tree algorithm (BDT) is used, combining variables related to lepton kinematics and \vec{p}_T^{miss} . The BDT is trained on simulated samples separately for different jet multiplicity categories, and the output discriminator is used to define a phase space enriched in signal events and reduced DY background contamination.

Events are required to pass the single-lepton or dilepton triggers. For each event, this analysis requires at least two high- p_T lepton candidates with opposite sign, originating from the primary vertex, categorized as dielectron, dimuon, or $e\mu$ pairs. Only jets with $p_T > 30$ GeV (20 GeV for b jets) and $|\eta| < 4.7$ ($|\eta| < 2.4$ for b jets) are considered in the analysis. Jets are ignored if they overlap with an isolated lepton within a distance of $\Delta R = 0.3$. In addition, the following kinematic selection is applied in the $e\mu$ final state: one electron and one muon are required to be reconstructed in the event with a minimum p_T of 13 GeV for the electron and 10 GeV for the muon, the higher p_T threshold for the electron resulting from the trigger def-

initiation. One of the two leptons should also have a p_T greater than 25 GeV. In the case of SF e^+e^- and $\mu^+\mu^-$ final states, the leading lepton is required to have p_T greater than 25 GeV when it is an electron, or 20 GeV when it is a muon. The subleading electron is required to have p_T greater than 13 GeV, while for the muon a minimum p_T of 10 GeV is required. Both leptons are required to be well identified, isolated, and prompt.

Given the large background contribution from $t\bar{t}$ production in both DF and SF final states, events are further categorized based on the number of jets in the event, with the 0-jet category driving the sensitivity of the analysis. A categorization of the selected events is performed, targeting different production mechanisms and different flavor compositions of the WW decay products.

5 Analysis categories

5.1 Different-flavor ggH categories

The categories described in this section target the ggH production mechanism and select the DF $e\mu$ final state. The main background processes are the nonresonant WW, top quark (both single and pair production), DY to τ lepton pairs, and W+jets when a jet is misidentified as a lepton. Smaller background contributions come from WZ, ZZ, $V\gamma$, $V\gamma^*$, and triboson production. The WW background process can be distinguished from the signal by the different kinematic properties of the lepton system, since it is dominated by the on-shell W boson pairs that do not arise from a scalar resonance decay. The top quark background process is diluted by defining different categories that depend on the number of jets in the event, and reduced by vetoing any b-tagged jet with $p_T > 20$ GeV.

The W+jets contribution (also referred to as nonprompt lepton background), where one jet mimics the signature of an isolated prompt lepton, is an important background process especially in the 0- and 1-jet ggH-tagged DF categories. This background is reduced by taking advantage of the charge symmetry of the signal, and the charge asymmetry of the W+jets process, in which the production of W^+ is favored over W^- . Also, the fact that the probabilities for a jet to mimic an electron or a muon are different, and the fact that the misidentification rate is larger for lower- p_T leptons, are exploited. Following these physics motivations the 0- and 1-jet ggH-tagged DF categories are further split into four categories according to the lepton flavor, charge and p_T ordering: $e^+\mu^-$, $e^-\mu^+$, μ^+e^- , and μ^-e^+ , where the first lepton is the one with the higher p_T . In addition, the four categories are divided according to whether the subleading lepton p_T (p_{T2}) is above or below 20 GeV. This eight-fold partitioning of the 0- and 1-jet ggH-tagged categories provides an improvement in terms of the expected significance of about 15% with respect to the inclusive 0- and 1-jet categories.

To suppress background processes with three or more leptons in the final state, no additional identified and isolated leptons with $p_T > 10$ GeV are allowed in the events for the dilepton categories. The dilepton invariant mass ($m_{\ell\ell}$) is required to be higher than 12 GeV, to reject low-mass resonances and background that comes from events with multiple jets that all arise through the strong interaction (referred to the multijet background). To suppress the background arising from DY events decaying to a τ lepton pair, which subsequently decays to the $e\mu$ final state, and to suppress processes without genuine missing transverse momentum, a minimum p_T^{miss} of 20 GeV is required. In the two-lepton categories, the DY background is further reduced by requiring the dilepton p_T ($p_T^{\ell\ell}$) to be higher than 30 GeV, as on average $e\mu$ lepton pairs from $Z \rightarrow \tau^+\tau^-$ decays have lower p_T than the ones from $H \rightarrow WW$ decays. These selection criteria also reduce contributions from $H \rightarrow WW \rightarrow \tau\nu\tau\nu$ and $H \rightarrow \tau^+\tau^-$.

Finally, to further suppress contributions from $Z \rightarrow \tau^+ \tau^-$ and W +jets events, where the sub-leading lepton does not arise from a W boson decay, the transverse mass built with \vec{p}_T^{miss} and the subleading lepton, defined as:

$$m_T^{\ell 2, p_T^{\text{miss}}} = \sqrt{2p_{T2} p_T^{\text{miss}} [1 - \cos \Delta\phi(\ell 2, \vec{p}_T^{\text{miss}})]}, \quad (1)$$

is required to be greater than 30 GeV. Here $\Delta\phi(\ell 2, \vec{p}_T^{\text{miss}})$ is the azimuthal angle between the subleading lepton momentum and \vec{p}_T^{miss} .

Although the invariant mass of the Higgs boson cannot be reconstructed because of the undetected neutrinos, the expected kinematic properties of the Higgs boson production and decay can be exploited. The spin-0 nature of the SM Higgs boson results in the preferential emission of the two charged leptons in the same hemisphere. Moreover, the invariant mass of the two leptons in the signal is relatively small with respect to the one expected for a lepton pair arising from other processes, such as nonresonant WW and top quark production. On the other hand, several of the smaller remaining background processes, such as nonprompt leptons, $DY \rightarrow \tau^+ \tau^-$, and $V\gamma$ populate the same $m_{\ell\ell}$ phase space as the Higgs boson signal. These can be partially disentangled from the signal by reconstructing the Higgs boson transverse mass as:

$$m_T = \sqrt{2p_T^{\ell\ell} p_T^{\text{miss}} [1 - \cos \Delta\phi(\ell\ell, \vec{p}_T^{\text{miss}})]}, \quad (2)$$

where $\Delta\phi(\ell\ell, \vec{p}_T^{\text{miss}})$ is the azimuthal angle between the dilepton momentum and \vec{p}_T^{miss} . These additional background processes populate different regions of the two-dimensional plane in $m_{\ell\ell}$ and m_T . A shape analysis based on a two-dimensional binned template fit of $m_{\ell\ell}$ versus m_T is performed to extract the Higgs boson signal in the DF ggH categories.

The observed events as a function of $m_{\ell\ell}$ and m_T are shown in Figs. 1, 2, and 3, after the template fit to the $(m_{\ell\ell}, m_T)$ distribution. The 0- and 1-jet categories are split into $p_{T2} < 20$ GeV and $p_{T2} > 20$ GeV subcategories, to show the different purity of the two regions. In these figures the postfit number of events is shown, i.e., each signal and background process is normalized to the result of a simultaneous fit to all categories, assuming that the relative proportions for the different Higgs boson production mechanisms are those predicted by the SM. The events in each bin of one of the two variables are obtained by integrating over the other, and weighted using the ratio of fitted signal (S) to the sum of signal and background (S + B). $S/(S + B)$ ratio in each m_T bin. This ratio is then used to perform a weighted sum of the $m_{\ell\ell}$ distributions in each m_T bin. A similar weighting procedure is applied when merging the distributions of a given variable in different categories. The weighting procedure is used only for visualization purposes, and is not used for signal extraction.

The full list of DF ggH categories and their selection requirements is shown in Table 1.

5.2 Different-flavor VBF category

The VBF process is the second largest Higgs boson production mechanism at the LHC. This mode involves the production of a Higgs boson in association with two jets with large rapidity separations. After the common preselection, the VBF analysis requires events with exactly two jets with $p_T > 30$ GeV, a pseudorapidity separation ($|\Delta\eta_{jj}|$) between the two jets larger than 3.5, and an invariant mass (m_{jj}) greater than 400 GeV. The rejection of events with more than two jets reduces the $t\bar{t}$ background contribution without affecting the signal efficiency, thus improving the signal sensitivity. The VBF analysis is based on the shape of the $m_{\ell\ell}$ distribution, and is split into two signal regions, one with $400 < m_{jj} < 700$ GeV and the other with $m_{jj} > 700$ GeV, to profit from the higher purity of the $m_{jj} > 700$ GeV region. The post-fit signal and

Table 1: Analysis categorization and event requirements for the 0-, 1-, and 2-jet ggH-tagged categories in the DF dilepton final state. The phase spaces defined by the 0-, 1-, and 2-jet ggH-tagged requirements correspond to the events shown in Figs. 1, 2, and 3, respectively.

Category	Subcategory	Requirements
Preselection	—	$m_{\ell\ell} > 12 \text{ GeV}$, $p_{T1} > 25 \text{ GeV}$, $p_{T2} > 13 \text{ (10) GeV}$ for e (μ), $p_T^{\text{miss}} > 20 \text{ GeV}$, $p_T^{\ell\ell} > 30 \text{ GeV}$ no additional leptons with $p_T > 10 \text{ GeV}$ electron and muon with opposite charges
0-jet ggH-tagged	$\left. \begin{array}{l} e^+ \mu^- \\ e^- \mu^+ \\ \mu^+ e^- \\ \mu^- e^+ \end{array} \right\} p_{T2} > 20 \text{ GeV}$	$m_T > 60 \text{ GeV}$, $m_T^{\ell 2, p_T^{\text{miss}}} > 30 \text{ GeV}$ subleading lepton $p_T > 20 \text{ GeV}$ no jets with $p_T > 30 \text{ GeV}$ no b-tagged jets with p_T between 20 and 30 GeV
	$\left. \begin{array}{l} e^+ \mu^- \\ e^- \mu^+ \\ \mu^+ e^- \\ \mu^- e^+ \end{array} \right\} p_{T2} < 20 \text{ GeV}$	$m_T > 60 \text{ GeV}$, $m_T^{\ell 2, p_T^{\text{miss}}} > 30 \text{ GeV}$ subleading lepton $p_T < 20 \text{ GeV}$ no jets with $p_T > 30 \text{ GeV}$ no b-tagged jets with p_T between 20 and 30 GeV
1-jet ggH-tagged	$\left. \begin{array}{l} e^+ \mu^- \\ e^- \mu^+ \\ \mu^+ e^- \\ \mu^- e^+ \end{array} \right\} p_{T2} > 20 \text{ GeV}$	$m_T > 60 \text{ GeV}$, $m_T^{\ell 2, p_T^{\text{miss}}} > 30 \text{ GeV}$ subleading lepton $p_T > 20 \text{ GeV}$ exactly one jet with $p_T > 30 \text{ GeV}$ no b-tagged jets with $p_T > 20 \text{ GeV}$
	$\left. \begin{array}{l} e^+ \mu^- \\ e^- \mu^+ \\ \mu^+ e^- \\ \mu^- e^+ \end{array} \right\} p_{T2} < 20 \text{ GeV}$	$m_T > 60 \text{ GeV}$, $m_T^{\ell 2, p_T^{\text{miss}}} > 30 \text{ GeV}$ subleading lepton $p_T < 20 \text{ GeV}$ exactly one jet with $p_T > 30 \text{ GeV}$ no b-tagged jets with $p_T > 20 \text{ GeV}$
2-jet ggH-tagged	$e\mu$	at least two jets with $p_T > 30 \text{ GeV}$ $m_T^{\ell 2, p_T^{\text{miss}}} > 30 \text{ GeV}$ and $m_T > 60 \text{ GeV}$ no b-tagged jets with $p_T > 20 \text{ GeV}$ $m_{jj} < 65 \text{ GeV}$ or $105 < m_{jj} < 400 \text{ GeV}$

background events as functions of $m_{\ell\ell}$ are shown in Fig. 4, for the two m_{jj} regions separately. The list of event requirements applied in this category is presented in Table 2.

5.3 Different-flavor VH with two jets category

The VH process involves the production of a Higgs boson in association with a W or Z boson. The 2-jet VH-tagged category targets final states where one vector boson (W or Z) decays into two resolved jets. This category with hadronically decaying vector bosons is affected by large backgrounds compared to the leptonic decays, but profits from a higher branching fraction. The 2-jet VH-tagged analysis reverses the pseudorapidity separation requirement of the VBF selection ($|\Delta\eta| < 3.5$) and requires m_{jj} to be between 65 and 105 GeV. In addition, the two leading jets are required to be central ($|\eta| < 2.5$) to profit from more stringent b jet veto requirements, given that b tagging can only be performed for central jets. A cut on $\Delta R_{\ell\ell} < 2$ is applied to suppress $t\bar{t}$ background, taking advantage of the spin-0 nature of the Higgs boson that results in leptons being preferentially emitted in nearby directions. This kinematic property is further enhanced in this category due to the boost of the Higgs boson recoiling against the associated vector boson.

The analysis is based on the shape of the $m_{\ell\ell}$ discriminant distribution, presented in Fig. 5. The

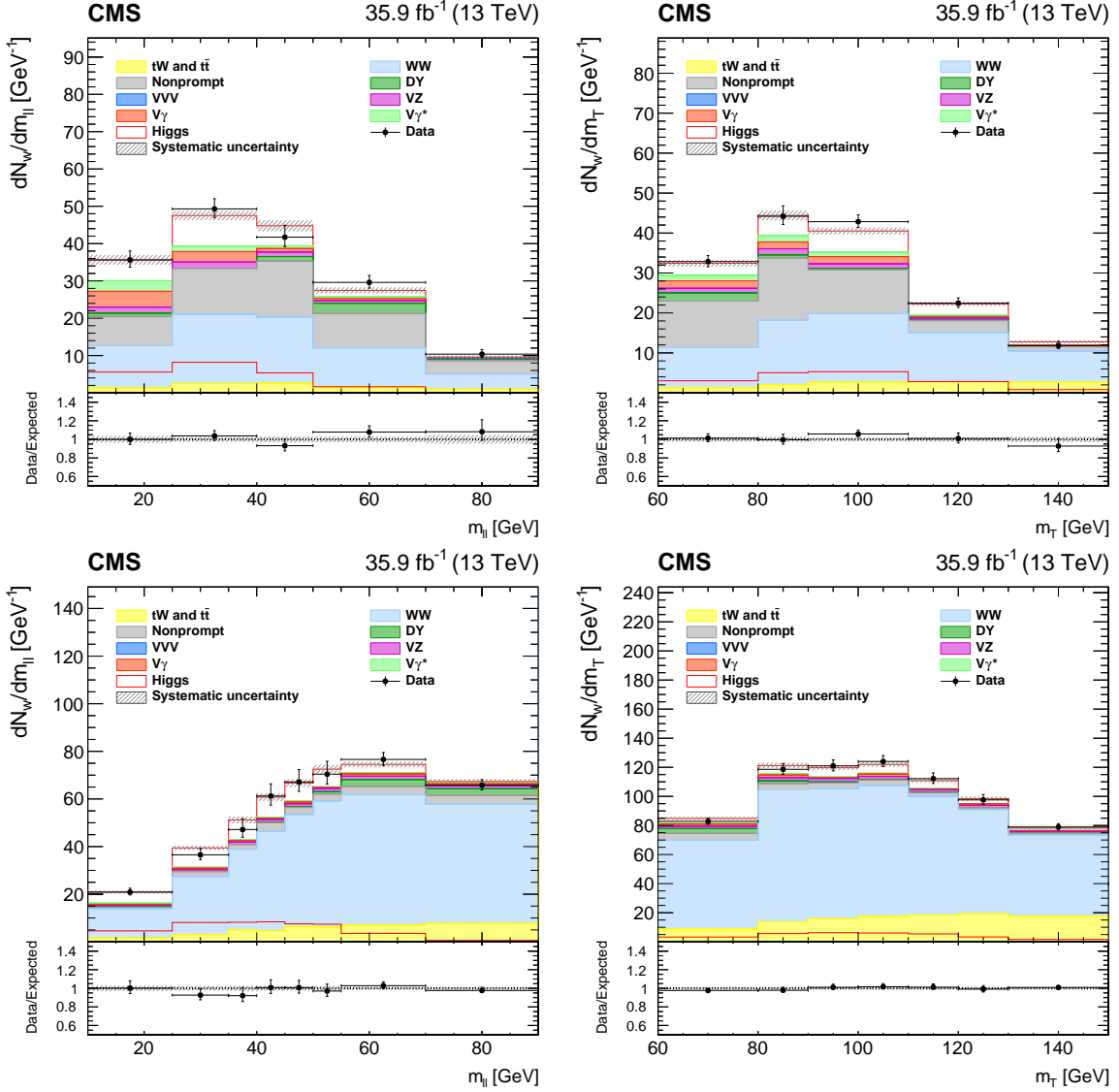


Figure 1: Postfit number of weighted events (N_w) as a function of $m_{\ell\ell}$ and m_T for DF events with 0 jets and $p_{T2} < 20$ GeV (upper row) or $p_{T2} > 20$ GeV (lower row). The number of events is weighted according to the $S/(S+B)$ ratio in each bin of one of the two variables, integrating over the other one. The various lepton flavor and charge subcategories are also merged and weighted according to their $S/(S+B)$ value. The contributions of the main background processes (stacked histograms) and the Higgs boson signal (superimposed and stacked red histograms) remaining after all selection criteria are shown. The dashed gray band accounts for all systematic uncertainties on the signal and background yields after the fit.

list of event requirements applied is presented in Table 3.

5.4 Same-flavor ggH categories

Similarly to the DF ggH-tagged analysis described in Section 5.1, an analysis targeting ggH in the SF e^+e^- and $\mu^+\mu^-$ channels is performed. The main challenge in this final state is the large DY background contribution. In order to control it, a BDT is trained to build a discriminator, called DYMVA, to identify DY events.

A categorization based on the p_T of the subleading lepton is introduced to better control the

Table 2: Analysis categorization and event requirements for the 2-jet VBF-tagged category, in the DF dilepton final state. The phase spaces defined by the 2-jet VBF-tagged requirements correspond to the events shown in Fig. 4.

Category	Subcategory	Requirements
Preselection	—	$m_{\ell\ell} > 12 \text{ GeV}$, $p_{T1} > 25 \text{ GeV}$, $p_{T2} > 13 \text{ (10) GeV}$ for $e(\mu)$, $p_T^{\text{miss}} > 20 \text{ GeV}$, $p_T^{\ell\ell} > 30 \text{ GeV}$ no additional leptons with $p_T > 10 \text{ GeV}$ electron and muon with opposite charges
		exactly two jets with $p_T > 30 \text{ GeV}$ $60 < m_T < 125 \text{ GeV}$ leptons η between the two leading jets $400 < m_{jj} < 700 \text{ GeV}$ and $ \Delta\eta_{jj} > 3.5$ no b-tagged jets with $p_T > 20 \text{ GeV}$
2-jet VBF-tagged	$e\mu$ low m_{jj}	exactly two jets with $p_T > 30 \text{ GeV}$ $60 < m_T < 125 \text{ GeV}$ leptons η between the two leading jets $400 < m_{jj} < 700 \text{ GeV}$ and $ \Delta\eta_{jj} > 3.5$ no b-tagged jets with $p_T > 20 \text{ GeV}$
	$e\mu$ high m_{jj}	exactly two jets with $p_T > 30 \text{ GeV}$ $60 < m_T < 125 \text{ GeV}$ leptons η between the two leading jets $m_{jj} > 700 \text{ GeV}$ and $ \Delta\eta_{jj} > 3.5$ no b-tagged jets with $p_T > 20 \text{ GeV}$

Table 3: Analysis categorization and event requirements for the 2-jet VH-tagged category, in the DF dilepton final state. The phase space defined by the 2-jet VH-tagged requirements corresponds to the events shown in Fig. 5.

Category	Subcategory	Requirements
Preselection	—	$m_{\ell\ell} > 12 \text{ GeV}$, $p_{T1} > 25 \text{ GeV}$, $p_{T2} > 13 \text{ (10) GeV}$ for $e(\mu)$ $p_T^{\text{miss}} > 20 \text{ GeV}$, $p_T^{\ell\ell} > 30 \text{ GeV}$ no additional leptons with $p_T > 10 \text{ GeV}$ electron and muon with opposite charges
		at least two jets with $p_T > 30 \text{ GeV}$ two leading jets with $ \eta < 2.5$ $60 < m_T < 125 \text{ GeV}$ and $\Delta R_{\ell\ell} < 2$ no b-tagged jets with $p_T > 20 \text{ GeV}$ $65 < m_{jj} < 105 \text{ GeV}$ and $ \Delta\eta_{jj} < 3.5$
2-jet VH-tagged	$e\mu$	at least two jets with $p_T > 30 \text{ GeV}$ two leading jets with $ \eta < 2.5$ $60 < m_T < 125 \text{ GeV}$ and $\Delta R_{\ell\ell} < 2$ no b-tagged jets with $p_T > 20 \text{ GeV}$ $65 < m_{jj} < 105 \text{ GeV}$ and $ \Delta\eta_{jj} < 3.5$

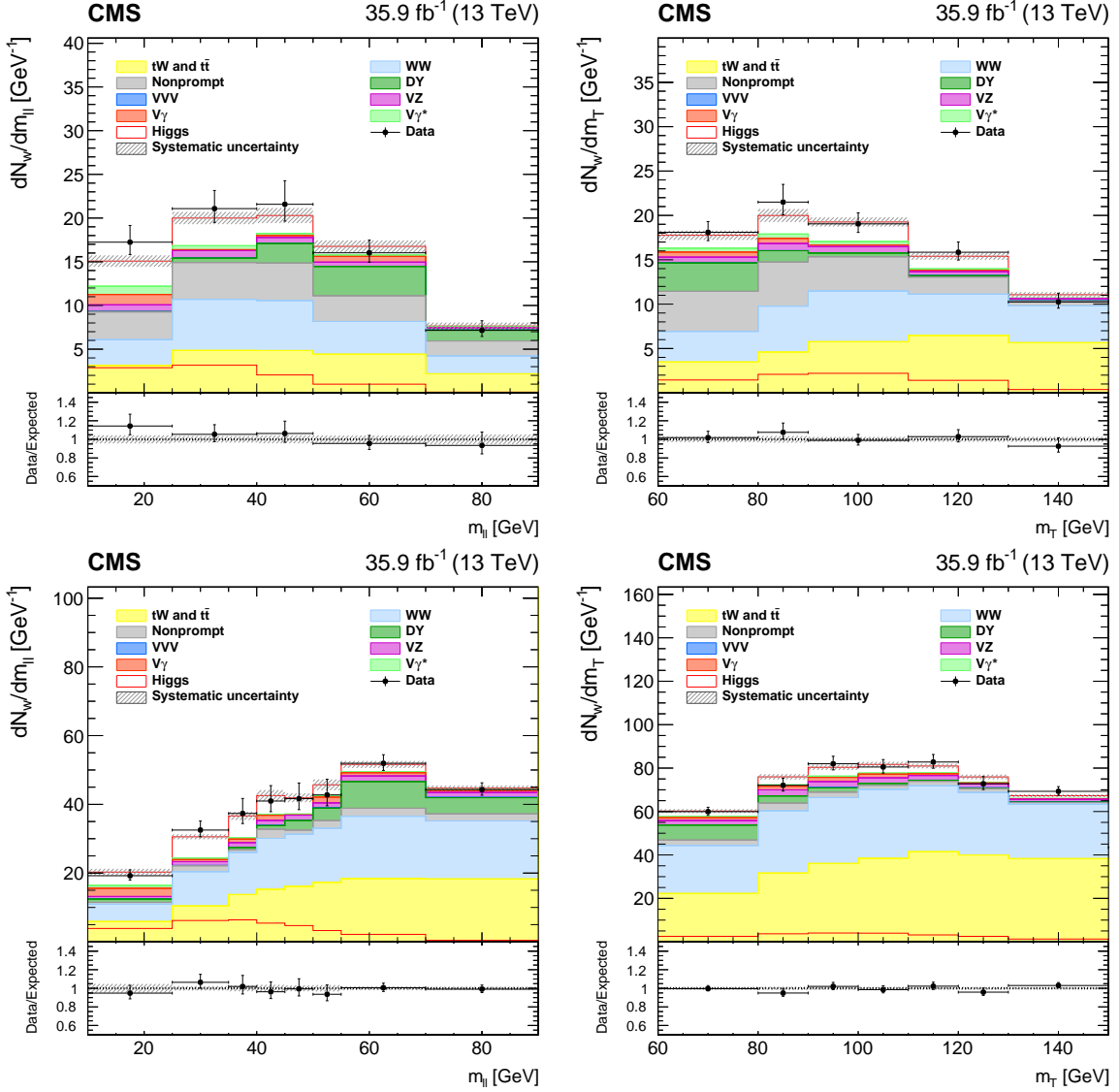


Figure 2: Same as previous figure, for DF events with one jet.

nonprompt lepton background, and a categorization in the number of jets is used to control the top quark backgrounds. The full list of event requirements is shown in Table 4.

This is an event-counting analysis, and the event requirements are chosen to maximize the expected signal significance in each category. The DY background estimations in these channels are based exclusively on control samples in data, as described in Section 6.

5.5 Associated WH production with three leptons in the final state

The three-lepton WH-tagged analysis selects events that have the leading lepton with $p_{T1} > 25$ GeV, the subleading lepton with $p_{T2} > 20$ GeV, and the trailing lepton with $p_{T3} > 15$ GeV. Events with a fourth lepton with $p_T > 10$ GeV are discarded. A veto is applied to events with SF lepton pairs of opposite charge that are compatible with coming from the decay of a Z boson. Events containing jets with $p_T > 30$ GeV or b-tagged jets with $p_T > 20$ GeV are also vetoed, to suppress the $t\bar{t}$ background. The azimuthal angle between \vec{p}_T^{miss} and the three-lepton system p_T , $\Delta\phi(\ell\ell\ell, \vec{p}_T^{\text{miss}})$, is used to reduce the contamination of nonprompt lepton backgrounds. The rest of the three-lepton WH-tagged selection is in common with the other categories. These

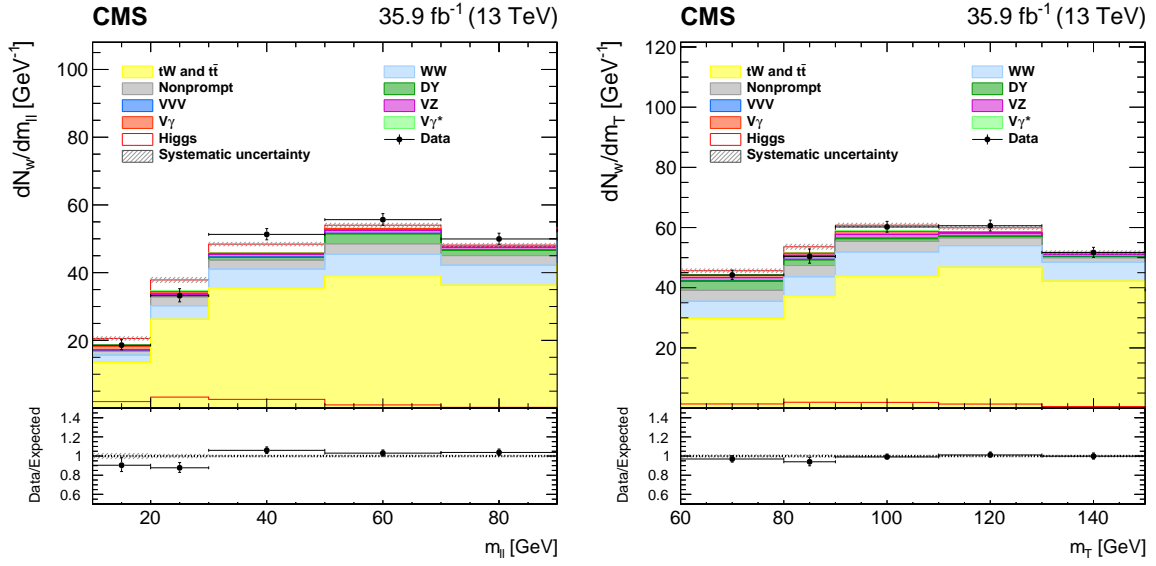


Figure 3: Postfit number of weighted events (N_w) as a function of $m_{\ell\ell}$ and m_T for DF events with at least 2 jets. The number of events is weighted according to the $S/(S+B)$ ratio in each bin of one of the two variables, integrating over the other one.

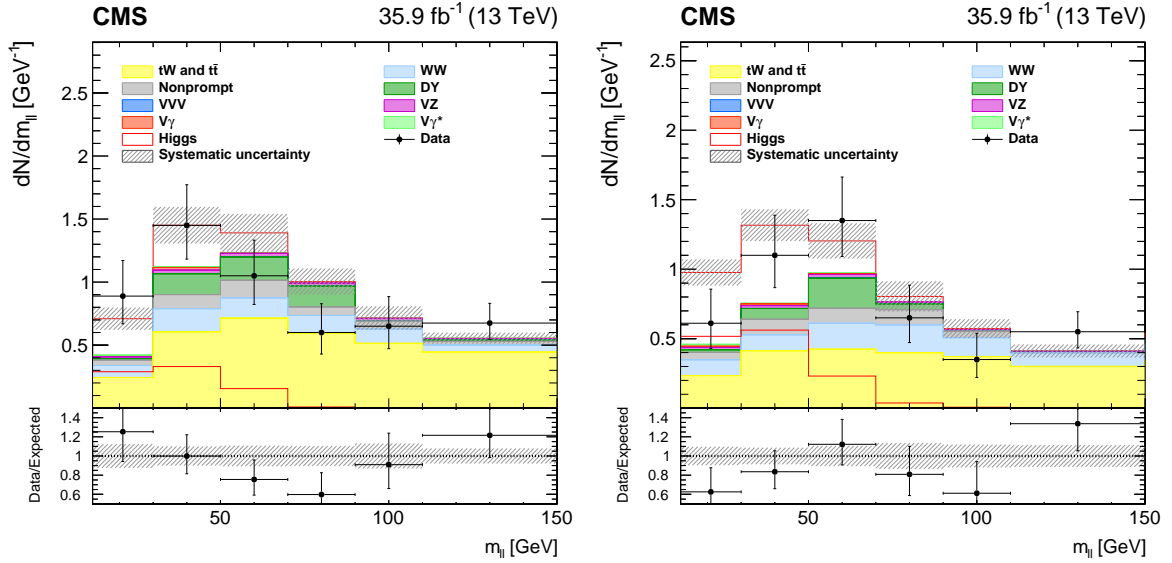


Figure 4: Postfit number of events with VBF topology as a function of $m_{\ell\ell}$, for $400 < m_{jj} < 700$ GeV (left) and $m_{jj} > 700$ GeV (right).

requirements are summarized in Table 5.

The events are further divided into two categories: same-sign SF (SSSF) lepton pairs, $\mu^\pm\mu^\pm e^\mp/e^\pm e^\pm\mu^\mp$, and opposite-sign SF (OSSF) lepton pairs, $\mu^\mp\mu^\pm e^\mp/e^\mp e^\pm\mu^\mp$. The two selections have different signal-over-background ratios, with the SSSF being the purest of the two. The main background contribution in both cases is the contamination from nonprompt leptons. In the OSSF category, events are required to have $p_T^{\text{miss}} > 50$ GeV to reduce the DY background.

The analysis is based on the minimum ΔR between oppositely charged leptons. The distribution of this variable is presented in Fig. 6, separately for the SSSF and OSSF categories.

Table 4: Analysis categorization and selections for the 0- and 1- jet ggH-tagged categories in the SF dilepton final state.

Category	Subcategory	Requirements
Preselection	—	$m_{\ell\ell} > 12 \text{ GeV}$, $p_{T1} > 25 \text{ (20) GeV}$ for e (μ), $p_{T2} > 13 \text{ (10) GeV}$ for e (μ), track $p_T^{\text{miss}} > 20 \text{ GeV}$, $p_T^{\ell\ell} > 30 \text{ GeV}$ no additional leptons with $p_T > 10 \text{ GeV}$ two electrons or two muons with opposite charges
0-jet ggH-tagged	e^+e^- $p_{T2} < 20 \text{ GeV}$ $\mu^+\mu^-$ $p_{T2} < 20 \text{ GeV}$	DYMVA > 0.991 , $m_{\ell\ell} < 55 \text{ GeV}$, $m_T > 50 \text{ GeV}$, $p_{T2} < 20 \text{ GeV}$, $\Delta\phi_{\ell\ell} < 1.7$ no jets with $p_T > 30 \text{ GeV}$ no b-tagged jets with $p_T > 20 \text{ GeV}$
	e^+e^- $p_{T2} > 20 \text{ GeV}$ $\mu^+\mu^-$ $p_{T2} > 20 \text{ GeV}$	DYMVA > 0.991 , $m_{\ell\ell} < 55 \text{ GeV}$, $m_T > 50 \text{ GeV}$, $20 \text{ GeV} < p_{T2} < 50 \text{ GeV}$, $\Delta\phi_{\ell\ell} < 1.7$ no jets with $p_T > 30 \text{ GeV}$ no b-tagged jets with $p_T > 20 \text{ GeV}$
1-jet ggH-tagged	e^+e^- $\mu^+\mu^-$	DYMVA > 0.95 , $m_{\ell\ell} < 57 \text{ GeV}$, $50 < m_T < 155 \text{ GeV}$, $p_{T1} < 50 \text{ GeV}$, $\Delta\phi_{\ell\ell} < 1.75$ exactly one jet with $p_T > 30 \text{ GeV}$ no b-tagged jets with $p_T > 20 \text{ GeV}$

Table 5: Analysis categorization and event requirements for the WH-tagged category, in the three-lepton final state. Here, $\min-m_{\ell+\ell-}$ is the minimum $m_{\ell\ell}$ between the oppositely charged leptons. For the Z boson veto, the opposite-sign same-flavor pair with the $m_{\ell\ell}$ closest to the Z boson mass is considered. Events that fulfill the three-lepton WH-tagged requirements correspond to the signal phase space shown in Fig. 6.

Category	Subcategory	Requirements
Preselection	—	$p_{T1} > 25 \text{ GeV}$, $p_{T2} > 20 \text{ GeV}$, $p_{T3} > 15 \text{ GeV}$ no additional leptons with $p_T > 10 \text{ GeV}$ $\min-m_{\ell+\ell-} > 12 \text{ GeV}$, total lepton charge sum ± 1
3-lepton WH-tagged	OSSF	no jets with $p_T > 30 \text{ GeV}$ no b-tagged jets with $p_T > 20 \text{ GeV}$ $p_T^{\text{miss}} > 50 \text{ GeV}$, $\min-m_{\ell+\ell-} < 100 \text{ GeV}$ Z boson veto: $ m_{\ell\ell} - m_Z > 25 \text{ GeV}$ $\Delta\phi(\ell\ell, \vec{p}_T^{\text{miss}}) > 2.2$
	SSSF	no jets with $p_T > 30 \text{ GeV}$ no b-tagged jets with $p_T > 20 \text{ GeV}$ $\Delta\phi(\ell\ell, \vec{p}_T^{\text{miss}}) > 2.5$

5.6 Associated ZH production with four leptons in the final state

The ZH final state is targeted by requiring exactly four isolated leptons with tight identification criteria and zero total charge, and large p_T^{miss} from the undetected neutrinos. The major background processes are ZZ and $t\bar{t}Z$ production.

Among the four leptons, the pair of SF leptons with opposite charge, and with the invariant mass closest to the Z boson mass, is chosen as the Z boson candidate. The remaining dilepton system, denoted as X, can be either SF or DF. Events are therefore divided into two categories, distinguishing between the cases in which the X candidate contains two DF leptons (XDF) or two SF leptons (XSF), as shown in Table 6.

The signal fraction is equally distributed in the two regions. In the XSF region, ZZ, DY, and $t\bar{t}Z$ production are the major background sources, while in the XDF region, $t\bar{t}Z$ and ZZ back-

Table 6: Analysis categorization and event requirements for the ZH-tagged category, in the four-lepton final state. Here, X is defined as the remaining lepton pair after the Z boson candidate is chosen. The component leptons of X can be either same-flavor (XSF) or different-flavor (XDF).

Category	Subcategory	Requirements
Preselection	—	four tight and isolated leptons, with zero total charge $p_T > 25$ GeV for the leading lepton $p_T > 15$ GeV for the second leading lepton $p_T > 10$ GeV for the remaining two leptons no additional leptons with $p_T > 10$ GeV Z dilepton mass > 4 GeV X dilepton mass > 4 GeV no b-tagged jets with $p_T > 20$ GeV
		4-lepton ZH-tagged
	XSF	$ m_{\ell\ell} - m_Z < 15$ GeV $10 < m_X < 50$ GeV $35 < p_T^{\text{miss}} < 100$ GeV four-lepton invariant mass > 140 GeV
	XDF	$ m_{\ell\ell} - m_Z < 15$ GeV $10 < m_X < 70$ GeV $p_T^{\text{miss}} > 20$ GeV

grounds are dominant. Backgrounds with two Z bosons fall predominantly into the XSF region, and enter the XDF selection only through the leptonic decays of the τ leptons. This makes the XDF region much cleaner than the XSF one.

Given the low expected signal yields in the XDF and XSF categories, the result in this case is extracted from event-counting in each category.

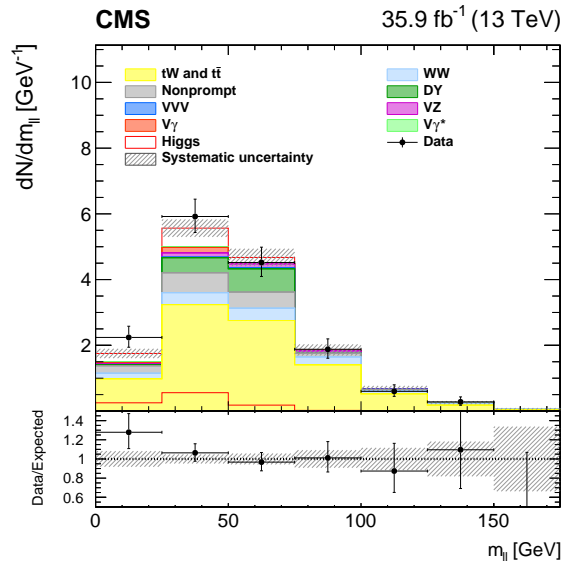


Figure 5: Postfit number of events as a function of $m_{\ell\ell}$ for DF events in the 2-jets VH-tagged category.

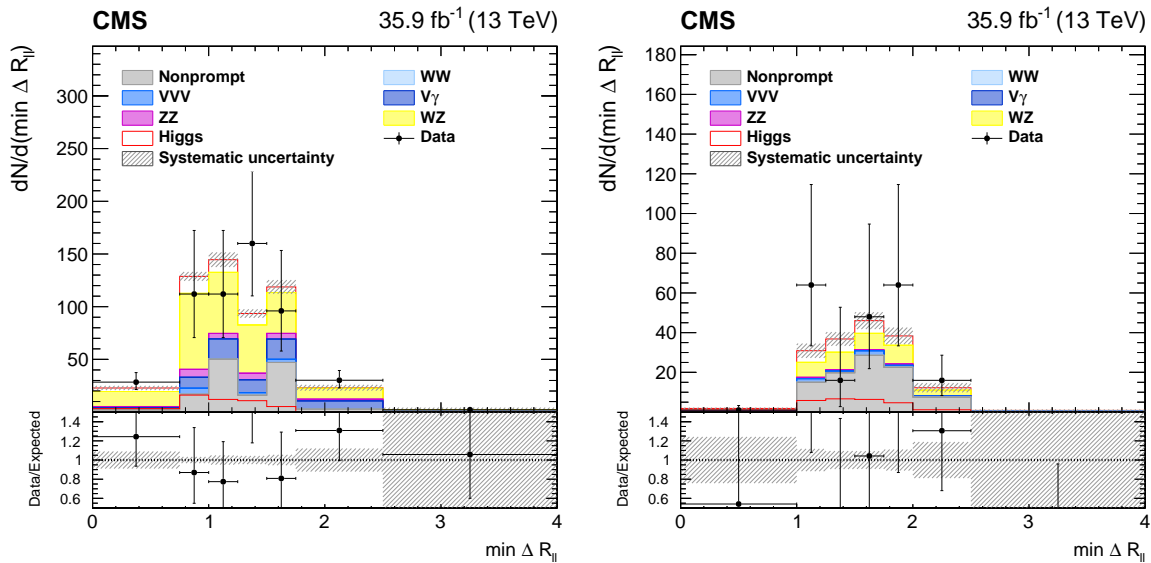


Figure 6: Postfit $\Delta R_{\ell\ell}$ distribution for events in the three-lepton WH-tagged category, split into the OSSF (left) and SSSF (right) subcategories.

6 Background estimation

6.1 Nonprompt lepton background

Events in which a single W boson is produced in association with jets may populate the signal region when a jet is misidentified as a lepton. These events contain a genuine lepton and p_T^{miss} from the W boson decay as well as a second nonprompt lepton from a misidentified jet, likely arising from a B hadron decay. A similar background arises from semileptonic decays of top quark pairs, especially in the 1- and 2- jets categories. At a lower rate, multijet production and fully hadronic top quark pair decays also contribute. These backgrounds are particularly important for events with low- p_T leptons and low $m_{\ell\ell}$, and hence in the signal region of the analysis.

The nonprompt lepton background is suppressed by the identification and isolation requirements imposed on the electrons and muons, while the remaining contribution is estimated directly from data. A control sample is defined using events in which one lepton passes the standard lepton identification and isolation criteria and another lepton candidate fails these criteria but passes a looser selection, resulting in a sample of “pass-fail” lepton pairs. The pass-fail sample is dominated by nonprompt leptons. The efficiency (ϵ_{misID}) for a jet that satisfies this looser selection to pass the standard selection is estimated directly from data in an independent sample dominated by events with nonprompt leptons from multijet processes. The contamination of prompt leptons from electroweak processes in such a sample is removed using the simulation. The uncertainty from this subtraction is propagated to ϵ_{misID} . The efficiency ϵ_{misID} is parameterized as a function of the p_T and η of the leptons, and is used to weight the events in the pass-fail sample by $\epsilon_{\text{misID}}/(1 - \epsilon_{\text{misID}})$, to obtain the estimated contribution from this background in the signal region. The contamination of prompt leptons in the “pass-fail” sample is corrected for using their probability to pass the standard selection given that they pass the looser selection, as measured in a Drell–Yan data control sample. The systematic uncertainty associated with the determination of ϵ_{misID} is dominant and arises from the dependence of ϵ_{misID} on the composition of the jet that is misidentified as a lepton. Its impact is estimated in two independent ways, which are combined to yield a conservative result. First, a closure test performed on simulated W +jets events with ϵ_{misID} estimated from simulated QCD multijet

events provides an overall normalization uncertainty. Second, a shape uncertainty is derived by varying the jet p_T threshold in the differential measurement of ϵ_{misID} in bins of the η and p_T of the lepton. The threshold is varied by a quantity that reflects the difference in the fake lepton p_T spectrum between $W+\text{jets}$ and $t\bar{t}$ events. The total uncertainty in ϵ_{misID} , including the statistical precision of the control sample, is about 40%. This uncertainty fully covers any data/simulation differences in control regions in which two same-sign leptons are requested.

6.2 Top quark background

Background contamination from single top quark processes, in particular tW associated production, and from $t\bar{t}$ production, arises because of the inefficiency of b jet identification and the relatively large top quark cross sections at 13 TeV. The shapes of the top quark background distributions in the various categories are obtained from simulation, taking into account the measured b jet identification inefficiencies. The normalizations are obtained from control regions enriched in top quark events. The background estimation is obtained separately for the 0-, 1- and 2-jet ggH-tagged categories, the 2-jet VBF- and VH-tagged categories, and for DF and SF final states.

The control region for the 0-jet ggH-tagged category is defined the same way as the signal region, except for the requirement that at least one jet with $20 < p_T < 30$ GeV is identified as a b jet by means of the b tagging algorithm. For the 1-jet ggH-tagged top quark enriched region, exactly one jet with $p_T > 30$ GeV identified as a b jet is required. In the 2-jet top quark enriched regions (either ggH-, VH-, or VBF-tagged), two jets with $p_T > 30$ GeV must be present in the event and at least one has to be identified as a b jet. To reduce other backgrounds in the top quark control regions, the dilepton mass is required to be higher than 50 GeV. The derived scale factors are shown in Table 7. The normalization of the top quark background in the three- and four-lepton categories is taken from simulation with its NNLO cross section uncertainty.

Table 7: Data-to-simulation scale factors for the top quark background normalization in seven different control regions.

Final state	Category	Scale factor
DF	0-jet ggH-tagged	0.94 ± 0.05
	1-jet ggH-tagged	0.94 ± 0.03
	2-jet ggH-tagged	0.98 ± 0.02
	2-jet VH-tagged	0.98 ± 0.03
	2-jet VBF-tagged	1.01 ± 0.04
SF	0-jet ggH-tagged	1.03 ± 0.06
	1-jet ggH-tagged	0.98 ± 0.02

The top quark p_T in $t\bar{t}$ events is reweighted in simulated samples in order to have a better description of the p_T distribution observed in data, as described in previous CMS analyses [60]. The difference between applying this reweighting, or not, is taken as a systematic shape uncertainty. The theoretical uncertainty related to the single top quark and $t\bar{t}$ cross sections is also taken into account. It is evaluated by varying the ratio between the single top quark and $t\bar{t}$ cross section by its uncertainty, which is 8% at 13 TeV [18]. A 1% theoretical uncertainty arising from PDF uncertainties and QCD scale variations affects the uncertainty on the signal region to control region ratio. All the experimental uncertainties described in Section 7 are also included as uncertainties on the top quark background shape.

6.3 Drell–Yan background

The $DY \rightarrow \tau^+\tau^-$ background is relevant for DF categories and, like the signal, populates the low- m_T and low- $m_{\ell\ell}$ phase space. The kinematic variables of this background are predicted by the simulation after reweighting the Z boson p_T spectrum to match the distribution measured in the data. The normalization is estimated in data control regions by selecting events with $m_T < 60$ GeV and $30 < m_{\ell\ell} < 80$ GeV. Normalization scale factors are extracted, separately for the 0-, 1-, 2-jet ggH-tagged, the 2-jet VBF- and VH-tagged categories, and are shown in Table 8.

Table 8: Data-to-simulation scale factors for the $DY \rightarrow \tau^+\tau^-$ background normalization in the DF control regions.

Final state	Category	Scale factor
DF	0-jet ggH-tagged	0.94 ± 0.06
	1-jet ggH-tagged	1.02 ± 0.05
	2-jet ggH-tagged	0.99 ± 0.09
	2-jet VH-tagged	0.99 ± 0.13
	2-jet VBF-tagged	1.04 ± 0.16

The effect of missing higher-order corrections in the DY simulation is estimated by varying the renormalization and factorization scales by a factor of two up and down. This effect is treated as a shape uncertainty and amounts to 1–2% in the DY yield. A 2% theoretical uncertainty arising from PDF uncertainties and scale variations affects the uncertainty on the signal region to control region ratio. All experimental uncertainties described in Section 7 are considered as shape uncertainties for this background process.

In the SF categories, a dominant source of background is $DY \rightarrow e^+e^-$ and $DY \rightarrow \mu^+\mu^-$. The contribution of the DY background outside the Z boson mass region (dubbed the *out* region, which corresponds to the signal region of the analysis) is estimated by counting the number of events in the Z boson mass region in data (*in* region), subtracting the non-Z-boson contribution from it, and scaling the yield by a ratio $R_{\text{out/in}}$. This ratio is defined as the fraction of events outside and inside the Z boson mass region in Monte Carlo (MC) simulation, $R_{\text{out/in}} = N_{\text{out}}^{\text{MC}} / N_{\text{in}}^{\text{MC}}$.

The Z boson mass region is defined as $|m_{\ell\ell} - m_Z| < 7.5$ GeV. Such a tight mass window is chosen to reduce the non-Z-boson background contributions, which can be split into two categories. The first one is composed of the background processes, such as top quark pair and W^+W^- production, with equal decay rates into the four lepton-flavor final states (ee , $e\mu$, μe , and $\mu\mu$). Their contributions to the Z boson mass region in data, $N_{\ell\ell}^{\text{background|in}}$, can be estimated from the number of events in the $e^\pm\mu^\mp$ final state, $N_{e\mu}^{\text{in}}$, applying a correction factor that accounts for the differences in the detection efficiency between electrons and muons (k_{ee} and $k_{\mu\mu}$):

$$N_{\ell\ell}^{\text{background|in}} = \frac{1}{2} k_{\ell\ell} (N_{e\mu}^{\text{in}} - N_{e\mu}^{\text{in}}(\text{VV})), \quad (3)$$

where $\ell\ell$ stands for ee or $\mu\mu$. $N_{e\mu}^{\text{in}}(\text{VV})$ is the number of events, estimated from simulation, arising from WZ and ZZ decays and contributing to the $e\mu$ final state. The factor of 1/2 comes from the relative branching fraction between the $\ell\ell$ and $e\mu$ final states. The second category is composed of background processes, such as WZ and ZZ (denoted as VV) production, with subsequent decay mostly into SF final states via the on-shell Z boson, which are determined from simulation. The number of events arising from these background processes contributing to the same flavor final state is denoted as $N_{\ell\ell}^{\text{in}}(\text{VV})$.

Finally, the number of DY events in the signal region is estimated from the number of events in

the SF final state, $N_{\ell\ell}^{\text{in}}$, separately for electrons and muons according to the following formula:

$$N_{Z \rightarrow \ell\ell}^{\text{out}} = R_{\text{out/in}} \left(N_{\ell\ell}^{\text{in}} - N_{\ell\ell}^{\text{background|in}} - N_{\ell\ell}^{\text{in}}(\text{VV}) \right). \quad (4)$$

The difference of the $R_{\text{out/in}}$ values from the data and simulation is taken as a systematic uncertainty, and amounts to 10–25%.

6.4 The WZ and $W\gamma^*$ background

The $W\gamma^*$ EW production is included in the simulation as part of the WZ production, and the two processes are separated using a 4 GeV threshold on the Z/γ^* mass at the generator level. For the final states with two leptons, the WZ and $W\gamma^*$ processes may contribute to the signal region whenever one of the three leptons is not identified. Therefore, it is important to observe the process in data to validate the simulation.

The yield of the WZ background is measured in data by selecting events with three isolated leptons, two electrons and one muon ($ee\mu$), or two muons and one electron ($\mu\mu e$). The SF lepton pair is identified as the Z boson candidate, and its invariant mass is required to be within the Z boson mass window defined in Section 6.3. This phase space is used to derive a scale factor for the WZ simulation, which is found to be 1.14 ± 0.18 , from the weighted average of the scale factors in the $ee\mu$ and $\mu\mu e$ regions with their statistical uncertainties.

A $W\gamma^*$ -enriched control region is defined by selecting events with two muons with invariant mass below 4 GeV, likely arising from a γ^* decay, and a third isolated electron or muon passing a tight identification requirement. The dimuon invariant mass region close to the J/ψ resonance mass is discarded. This control region is used to derive a scale factor for the $W\gamma^*$ simulation, which is found to be 0.9 ± 0.2 , with the uncertainty coming from the event counts in the $\mu\mu e$ and $\mu\mu\mu$ samples.

All experimental uncertainties described in Section 7 are considered as shape and yield uncertainties for the WZ and $W\gamma^*$ background determination. Moreover the effects of scale and PDF uncertainties on the normalization (3% from scale variations and 4% for PDF variations) and acceptance (3%) are included.

6.5 Nonresonant WW and other backgrounds

The nonresonant WW background populates the entire two-dimensional phase space in $m_{\ell\ell}$ and m_T , while the Higgs boson signal is concentrated at low $m_{\ell\ell}$ values, and m_T values around the Higgs boson mass. The yield of this background is hence estimated directly from the fit procedure, separately for each category. The derived scale factors are shown in Table 9.

Table 9: Scale factors for the nonresonant WW background normalization.

Final state	Category	Scale factor
DF	0-jet ggH-tagged	1.16 ± 0.05
	1-jet ggH-tagged	1.05 ± 0.13
	2-jet ggH-tagged	0.8 ± 0.4
	2-jet VH-tagged	0.6 ± 0.6
	2-jet VBF-tagged	0.5 ± 0.5
SF	0-jet ggH-tagged	1.13 ± 0.07
	1-jet ggH-tagged	1.03 ± 0.18

In the $q\bar{q} \rightarrow WW$ process, the p_T^{WW} spectrum in simulation is reweighted to match the re-summed calculation [41, 42]. The modeling of the shape uncertainties related to missing higher

orders is done in two pieces: the first varies the factorization and renormalization scales by a factor of two up and down and takes the envelope; the second independently varies the resummation scale by a factor of two up and down. The cross section of the gluon-induced WW process is scaled to NLO accuracy and the uncertainty on this K factor is 15% [61]. In categories with at least two jets, the EW WW production is also taken into account. The theoretical uncertainty in the LO cross section of this process amounts to 11%, and is estimated by varying the renormalization and factorization scales by a factor of two up and down, including also the effect of PDF variations.

The WZ and $Z\gamma^*$ backgrounds in the three-lepton WH-tagged analysis are estimated using dedicated control regions from which the scale factors of 1.09 ± 0.06 and 1.61 ± 0.18 , respectively, are derived. The ZZ background in the four-lepton ZH-tagged analysis is also estimated using a control region from which a scale factor of 0.96 ± 0.07 is derived.

All remaining backgrounds from diboson and triboson production are estimated according to their expected theoretical cross sections and the shape is taken from simulation.

7 Statistical procedure and systematic uncertainties

The statistical methodology used to interpret subsets of data selected for the $H \rightarrow WW$ analysis and to combine the results from the independent categories has been developed by the ATLAS and CMS Collaborations in the context of the LHC Higgs Combination Group. A general description of the methodology can be found in Ref. [62].

The number of events in each category and in each bin of the discriminant distributions used to extract the signal is modeled as a Poisson random variable, with a mean value that is the sum of the contributions from the processes under consideration. Systematic uncertainties are represented by individual nuisance parameters with log-normal distributions. The uncertainties affect the overall normalizations of the signal and backgrounds, as well as the shapes of the predictions across the distributions of the observables. Correlations between systematic uncertainties in different categories are taken into account.

The various control regions described in Section 6 are used to constrain individual backgrounds and are included in the fit in the form of single bins, representing the number of events in each of the control regions.

The remaining sources of systematic uncertainties of experimental and theoretical nature are described below. Effects due to the experimental uncertainties are estimated by scaling or smearing the targeted variable in the simulation and recalculating the analysis results. All experimental sources of systematic uncertainty, except for the integrated luminosity, have both a normalization and a shape component. The following experimental uncertainties are taken into account:

- The uncertainty in the measured luminosity, which is 2.5% [63].
- The trigger efficiency uncertainty associated with the combination of single-lepton and dilepton triggers, which is 2% [64].
- The uncertainties in the lepton reconstruction and identification efficiencies, which vary within 2–5% for electrons [56] and 1–2% for muons [65], depending on p_T and η .
- The muon momentum and electron energy scale and resolution uncertainties, which amount to 0.6–1.0% for electrons and 0.2% for muons.

- The jet energy scale uncertainties, which vary in the range 1–13%, depending on the p_T and η of the jet [66].
- The p_T^{miss} resolution uncertainty includes the propagation of lepton and jet energy scale and resolution uncertainties to p_T^{miss} , as well as the uncertainties on the energy scales of particles that are not clustered into jets, and the uncertainty on the amount of energy coming from pileup interactions.
- The scale factors correcting the b tagging efficiency and mistagging rates, which are varied within their uncertainties. The associated systematic uncertainty, which varies between 0.5–1.0% [59], affects, in an anticorrelated way, the top quark control regions and the signal ones.

The uncertainties in the signal and background production rates due to the limited knowledge of the processes under study include several components, which are assumed to be independent: the choices of PDFs and the strong coupling constant α_S , the UE and parton shower model, and the effects of missing higher-order corrections via variations of the renormalization and factorization scales. As most of the backgrounds are estimated from control regions in data, these theoretical uncertainties mostly affect the Higgs boson signal and they are implemented as normalization-only uncertainties unless stated otherwise.

The PDFs and α_S uncertainties are further split between the cross section normalization uncertainties computed by the LHC Higgs Cross Section Working Group [38] for the Higgs boson signal and their effect on the acceptance [67]. The signal cross section normalization uncertainties amount to 3% for the ggH and 2% for the VBF Higgs boson production mechanism, between 1.6% and 1.9% for VH processes, and 3.6% for t \bar{t} H production. The acceptance uncertainties are less than 1% for all production mechanisms.

The effect of missing higher order QCD corrections on the ggH production mechanism is split into nine individual components as identified in Ref. [37], chapter I.4. Each component is propagated such that both the integrated effect and the correlations across different categories are properly taken into account. The overall effect on the ggH cross section is about 10%. The effect of missing higher-order corrections in the VBF and VH simulations is less than 1%, while it amounts to about 8% for the t \bar{t} H simulation.

The UE uncertainty is estimated by varying the CUET8PM1 tune in a range corresponding to the envelope of the single tuned parameters post-fit uncertainty, as described in Section 3. The dependence on the parton shower (PS) model is estimated by comparing samples processed with different programs, as described in Section 3. The effect on the expected ggH signal yields after preselection is about 5% for the UE tuning and about 7% for the PS description, and is partially accounted for by the lepton identification scale factors and uncertainties. The remaining contribution is migration between jet categories and is anticorrelated between the 0-jet category and the categories with jets. Such effects are of the order of 15–25% for the parton shower (VBF categories being the most affected) and 5–17% for UE (2-jet VH-tagged category being the most affected). The anticorrelation between jet categories reduces the impact of these uncertainties on the final results.

Finally, the uncertainties arising from the limited number of events in the simulated samples are included independently for each bin of the discriminant distributions in each category.

8 Results

The signal strength modifier (μ), defined as the ratio between the measured signal cross section and the SM expectation in the $H \rightarrow WW \rightarrow 2\ell 2\nu$ decay channel, is measured by performing a binned maximum likelihood fit using simulated binned templates for signal and background processes.

The combined results obtained using all the individual analysis categories are described in this section. A summary of the expected fraction of different signal production modes in each category is shown in Fig. 7, together with the total number of expected $H \rightarrow WW$ events. The chosen categorization proves effective in tackling the different production mechanisms, especially ggH, VBF, and VH. The measurements assume a Higgs boson mass of $m_H = 125.09$ GeV, as reported in the ATLAS and CMS combined Higgs boson mass measurement [14]. The results reported below show a very weak dependence on the Higgs boson mass hypothesis, with the expected signal yield varying within 1% when the signal mass hypothesis is varied within its measured uncertainty.

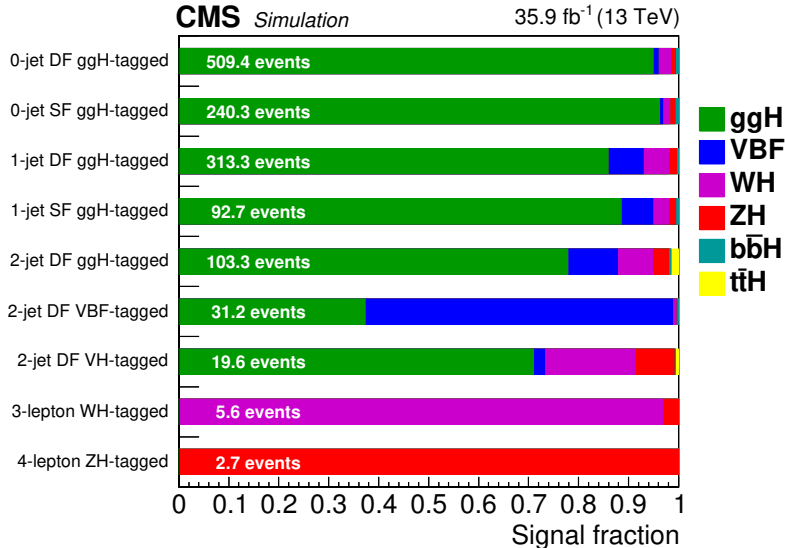


Figure 7: Expected relative fraction of different Higgs boson production mechanisms in each category included in the combination, together with the expected signal yield.

The number of expected signal and background events, and the number of observed events in data, in each category after the full event selection are shown in Tables 10 and 11. Postfit event yields are also shown in parentheses, and correspond to the result of a simultaneous fit to all categories, assuming that the relative proportions of the different production mechanisms are those predicted by the SM.

8.1 Signal strength modifiers

The signal strength modifier is extracted by performing a simultaneous fit to all categories assuming that the relative proportions of the different production mechanisms are the same as the SM ones. As such, the value of μ provides an insight into the compatibility between this measurement and the SM. The combined observed signal strength modifier is:

$$\mu = 1.28_{-0.17}^{+0.18} = 1.28 \pm 0.10 \text{ (stat)} \pm 0.11 \text{ (syst)}_{-0.07}^{+0.10} \text{ (theo)}, \quad (5)$$

where the statistical, systematic, and theoretical uncertainties are reported separately. The statistical component is estimated by fixing all the nuisance parameters to their best fit values and

Table 10: Number of expected signal and background events and number of observed events in the 0- and 1-jet categories after the full event selection. Postfit event yields are also shown in parentheses, corresponding to the result of a simultaneous fit to all categories assuming that the relative proportions for the different production mechanisms are those predicted by the SM. The individual signal yields are given for different production mechanisms. The total uncertainty accounts for all sources of uncertainty in signal and background yields after the fit.

	0-jet DF ggH-tagged	1-jet DF ggH-tagged	0-jet SF ggH-tagged	1-jet SF ggH-tagged
ggH	483.1 (642.1)	269.1 (339.3)	231.2 (324.6)	82.0 (92.8)
VBF	5.6 (7.4)	22.1 (29.4)	1.5 (2.5)	5.9 (9.3)
WH	12.4 (16.4)	15.8 (20.6)	3.3 (4.3)	2.9 (3.8)
ZH	5.2 (6.9)	5.0 (6.7)	2.6 (3.4)	1.4 (1.8)
ttH	<0.1 (<0.1)	0.2 (0.2)	<0.1 (<0.1)	<0.1 (<0.1)
bbH	3.4 (4.4)	1.5 (2.0)	1.7 (2.3)	0.5 (0.7)
Signal	509 (677)	313 (398)	240 (337)	93 (108)
±total unc.	(±31)	(±19)	(±24)	(±13)
WW	7851 (9088)	3553 (3727)	1596 (1805)	373 (365)
Top quark	2505 (2422)	5395 (5224)	334 (339)	452 (443)
Nonprompt	1555 (1006)	781 (482)	301 (260)	111 (97)
DY	154 (154)	283 (302)	437 (459)	178 (216)
VZ/V γ^*	368 (385)	327 (338)	101 (104)	43 (43)
V γ	213 (210)	137 (128)	23 (26)	17 (19)
Other diboson	5.1 (5.3)	3.5 (3.7)	9.3 (9.4)	2.0 (2.1)
Triboson	9.3 (9.6)	16 (17)	1.2 (1.2)	1.3 (1.3)
Background	12660 (13280)	10496 (10222)	2803 (3004)	1177 (1186)
±total unc.	(±141)	(±178)	(±97)	(±83)
Data	13964	10591	3364	1308

recomputing the likelihood profile. The breakdown of a given group of uncertainties (systematic or theoretical) is obtained by fixing all the nuisance parameters in the group to their best fit values, and recomputing the likelihood profile. The corresponding uncertainty is then taken as the difference in quadrature between the total uncertainty and the one obtained fixing the group of nuisance parameters. The expected and observed likelihood profiles as functions of the signal strength modifier are shown in Fig. 8, with the 68% and 95% confidence level (CL) indicated. The observed significance in the asymptotic approximation [68] of the Higgs boson production for the combination of all categories is 9.1 s.d., to be compared with the expected value of 7.1 s.d. As such, this is the first observation of the Higgs boson decay to W boson pairs with the CMS experiment.

A breakdown of the impact on μ of the different systematic uncertainties is shown in Table 12. The contributions of the normalizations that are left floating in the fit enter the statistical error on μ .

In order to assess the compatibility of the observed signal with the SM predictions in each category of the analysis and to ascertain the compatibility between the different categories, a simultaneous fit in which the signal strength modifier is allowed to float independently in each category is performed. The observed signal strength modifier for each category used in the combination is reported in Fig. 9 (left). Results are generally consistent with unity, with the largest deviation showing up in the 2-jet VH-tagged category (i.e., the category targeting the

Table 11: Number of expected signal and background events and number of observed events in the 2-jet, 3-lepton, and 4-lepton categories after the full event selection. Postfit event yields are also shown in parentheses, corresponding to the result of a simultaneous fit to all categories assuming that the relative proportions for the different production mechanisms are those predicted by the SM. The individual signal yields are given for different production mechanisms. For the 3-lepton WH-tagged category, the “Other diboson” background includes mainly WZ production, with a 10% contribution from ZZ events. For the 4-lepton ZH-tagged category, $t\bar{t}W$ and $t\bar{t}Z$ are included in the top quark process, while the “Other diboson” background mainly comes from ZZ production. The total uncertainty accounts for all sources of uncertainty in signal and background yields after the fit.

	2-jet DF ggH-tagged	2-jet DF VBF-tagged	2-jet DF VH-tagged	3-lepton WH-tagged	4-lepton ZH-tagged
ggH	80.4 (100.6)	11.6 (14.6)	13.9 (17.4)	<0.1 (<0.1)	<0.1 (<0.1)
VBF	10.3 (13.3)	19.2 (24.5)	0.4 (0.6)	<0.1 (<0.1)	<0.1 (<0.1)
WH	7.2 (9.3)	0.2 (0.2)	3.6 (4.6)	5.4 (7.2)	<0.1 (<0.1)
ZH	3.3 (4.3)	<0.1 (<0.1)	1.5 (2.1)	0.2 (0.2)	2.7 (3.5)
$t\bar{t}H$	1.6 (2.1)	<0.1 (<0.1)	0.1 (0.2)	<0.1 (<0.1)	<0.1 (<0.1)
$b\bar{b}H$	0.6 (0.7)	<0.1 (0.1)	<0.1 (<0.1)	<0.1 (<0.1)	<0.1 (<0.1)
Signal	103 (130)	31 (40)	20 (25)	5.6 (7.4)	2.7 (3.5)
\pm total unc.	(± 16)	(± 3)	(± 3)	(± 0.7)	(± 0.3)
WW	1048 (860)	69 (46)	52 (34)	<0.1 (<0.1)	<0.1 (<0.1)
Top quark	5197 (5187)	157 (158)	230 (229)	<0.1 (<0.1)	0.3 (0.3)
Nonprompt	359 (305)	30 (20)	42 (37)	19 (21)	<0.1 (<0.1)
DY	110 (112)	20 (19)	29 (30)	<0.1 (<0.1)	<0.1 (<0.1)
VZ/V γ^*	136 (137)	7.1 (6.9)	11 (10)	<0.1 (<0.1)	<0.1 (<0.1)
V γ	59 (53)	2.8 (2.8)	4.2 (4.6)	3.8 (9.6)	<0.1 (<0.1)
Other diboson	2.1 (2.3)	0.3 (0.3)	1.2 (1.3)	32 (37)	13 (13)
Triboson	15 (15)	0.3 (0.3)	2.0 (2.0)	2.1 (2.1)	0.4 (0.4)
Background	6926 (6671)	287 (253)	371 (348)	57 (70)	13.7 (13.7)
\pm total unc.	(± 502)	(± 17)	(± 37)	(± 7)	(± 0.6)
Data	6802	285	386	85	15

associated production of a Higgs boson with a vector boson decaying hadronically). The level of compatibility of the signal strength modifiers in each category with the combined signal

Table 12: Impact of the main systematic uncertainties on the signal strength μ .

Type	Source	Impact (%)
Theoretical	Signal	7
	WW	2
	Top quark	2
	PS and UE	2
	Sample size of simulation data	2
	Electrons	5
Experimental	Luminosity	4
	Muons	3
	b-tagging	3
	Nonprompt	3
	Jets	2
	p_T^{miss}	2
	VZ/V γ^* scale factor	2
	DY SF scale factor	2

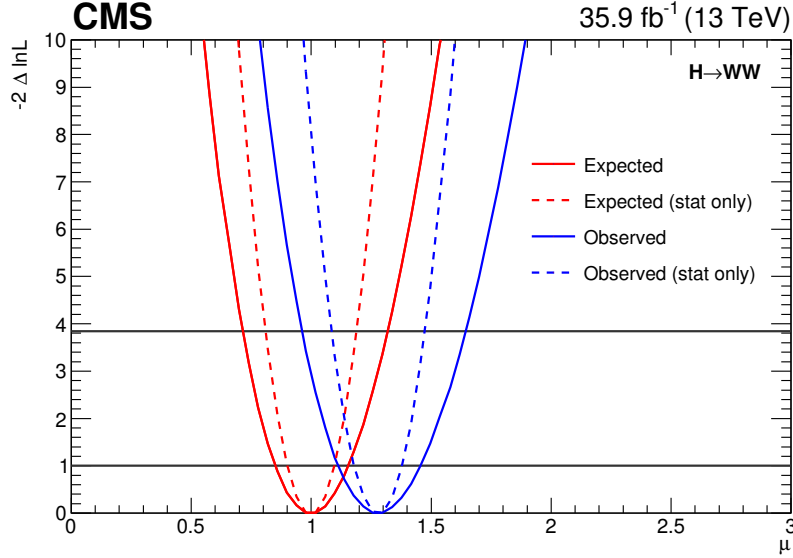


Figure 8: Observed and expected likelihood profiles for the global signal strength modifier. Dashed curves correspond to the likelihood profiles obtained including only the statistical uncertainty. The crossings with the horizontal line at $-2\Delta \ln L = 1$ (3.84) define the 68 (95)% CL interval.

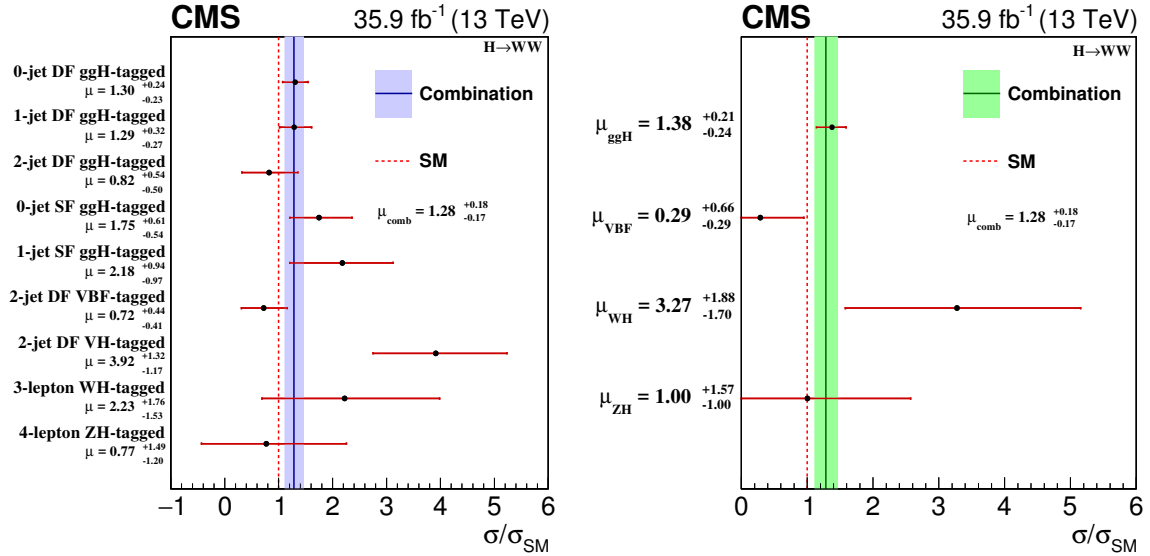


Figure 9: (Left) Observed signal strength modifiers for the categories used in the combination. (Right) Observed signal strength modifiers corresponding to the main SM Higgs boson production mechanisms, for a Higgs boson with a mass of 125.09 GeV. The vertical continuous line represents the combined signal strength best fit value, while the horizontal bars and the filled area show the 68% confidence intervals. The vertical dashed line corresponds to the SM expectation.

strength modifier corresponds to an asymptotic p -value of 0.34.

Given the sensitivity of the analysis to various production mechanisms, a fit is performed in which a different signal strength modifier is assigned to each production mechanism, i.e., μ_{ggH} , μ_{VBF} , μ_{WH} , and μ_{ZH} . A simultaneous fit to all categories is performed, and results are shown in

Fig. 9 (right). The biggest deviation from unity is observed for the WH production mechanism, which is probed mainly by the 2-jet VH-tagged and 3-lepton WH-tagged categories. The level of compatibility of the signal strength modifiers associated with different production mechanisms with the combined signal strength modifier corresponds to an asymptotic p -value of 0.70.

A similar simultaneous fit has been performed to measure the cross section corresponding to five Higgs boson production mechanisms, using a simplified fiducial phase space, as specified in the “stage-0” simplified template cross section framework [37]. The cross sections corresponding to five Higgs boson production processes (σ_{ggH} , σ_{VBF} , $\sigma_{\text{WH lep.}}$, $\sigma_{\text{ZH lep.}}$, $\sigma_{\text{VH had.}}$) are measured requiring the generator-level Higgs boson rapidity to be $|y_H| < 2.5$. This analysis has a negligible acceptance for Higgs boson production above $|y_H| = 2.5$. The $H \rightarrow \tau\tau$ events are considered as background in this fit. The measured cross sections and their ratio with the SM predictions, for the production channels in which the analysis has sensitivity, are shown in Fig. 10. The observed deviation of the $\sigma_{\text{VH had.}}$ process with respect to the SM prediction corresponds to an asymptotic p -value of 0.02, and is driven by the excess of events already observed for μ_{WH} . Compared to the μ_{WH} fit, in this case the signal strength modifier for the hadronic decay of the associated W boson is fitted separately from the leptonic one, and is driven away from the SM prediction by the excess observed in the 2-jet VH-tagged category.

8.2 Higgs boson couplings

Given its large cross section times branching fraction, the $H \rightarrow WW$ channel has the potential for constraining the Higgs boson couplings to vector bosons and fermions. A fit is performed to probe these couplings. One signal strength modifier (μ_F) is used to scale fermion-induced

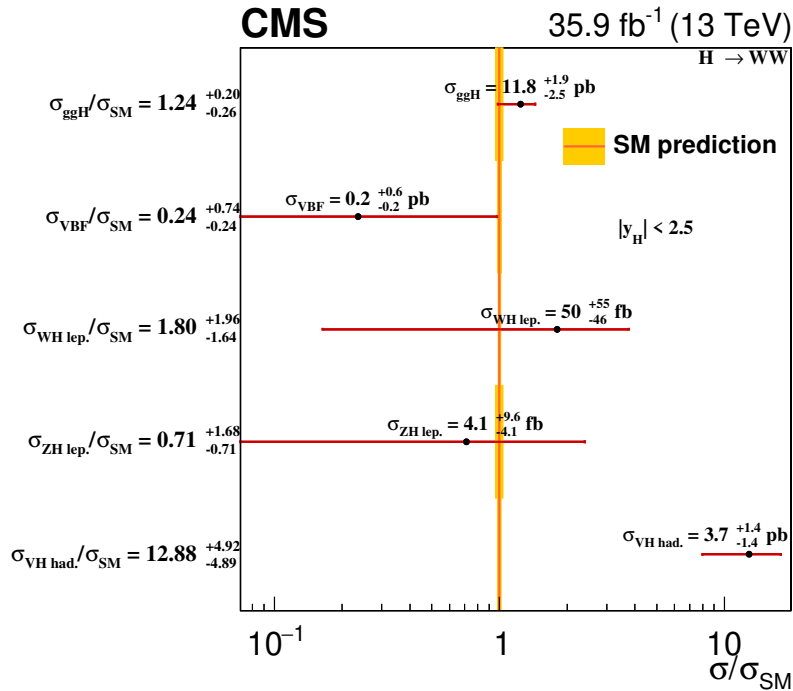


Figure 10: Observed cross sections and their ratio with the SM predictions for the main Higgs boson production modes. Cross section ratios are measured in a simplified fiducial phase space defined by requiring $y_H < 2.5$, as specified in the “stage-0” simplified template cross section framework [37]. The vertical line and band correspond to the SM prediction and associated theoretical uncertainty.

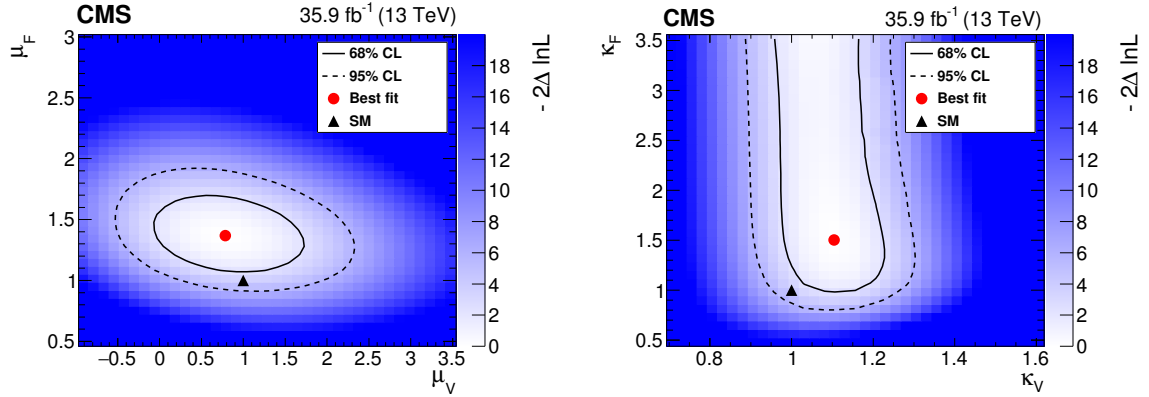


Figure 11: Two-dimensional likelihood profile as a function of (left) the signal strength modifiers associated with either fermion (μ_F) or vector boson (μ_V) couplings, and (right) the coupling modifiers associated with either fermion (κ_F) or vector boson (κ_V) vertices, using the κ -framework parametrization. The 68% and 95% CL contours are shown as continuous and dashed lines, respectively. The red circle represents the best fit value, while the black triangle corresponds to the SM prediction.

production mechanisms, i.e., ggH , $t\bar{t}H$, and $b\bar{b}H$, and another one (μ_V) scales the production mechanisms associated with vector bosons, i.e., VBF and VH. The two-dimensional likelihood profile is shown in Fig. 11 (left), where the 68% and 95% CL contours in the (μ_F, μ_V) plane are displayed. The best fit values for the signal strength modifiers are $\mu_F = 1.37^{+0.21}_{-0.20}$ and $\mu_V = 0.78^{+0.60}_{-0.57}$.

The determination of the Higgs boson coupling constants is a way to verify the theoretical predictions and to search for deviations with respect to the SM expectations. These couplings can be parametrized using two coupling modifiers associated either with fermion or vector boson vertices, using the so-called κ -framework [37]. The two coupling modifiers are used to scale the expected product of cross section and branching fraction to match the observed signal yields in the data, according to the following formula:

$$\sigma \mathcal{B}(X \rightarrow H \rightarrow WW) = \kappa_i^2 \frac{\kappa_V^2}{\kappa_H^2} \sigma_{\text{SM}} \mathcal{B}_{\text{SM}}(X \rightarrow H \rightarrow WW), \quad (6)$$

where $\kappa_H = \kappa_H(\kappa_F, \kappa_V)$ is the Higgs boson total width modifier, defined as a function of the two fit parameters κ_F and κ_V . The κ_i coupling modifier is equal to κ_F for the ggH , $t\bar{t}H$, and $b\bar{b}H$ production modes, and to κ_V for the VBF and VH production modes. No processes other than SM ones are considered to contribute to the total width modifier. The two-dimensional likelihood profile obtained using this approach, and the corresponding 68% and 95% CL contours, are shown in Fig. 11 (right). The best fit values for the coupling modifiers, obtained with one-dimensional fits in which the other coupling is profiled, are $\kappa_F = 1.52^{+0.48}_{-0.41}$ and $\kappa_V = 1.10^{+0.08}_{-0.08}$. The fact that κ_V is larger than 1 while the signal strength modifier μ_V is below 1 is due to the former being constrained not only by the production, but also by the decay of the Higgs boson, and thus being affected by the fact that the global observed signal strength is larger than 1.

9 Summary

Measurements of the properties of the SM Higgs boson decaying to a W boson pair at the LHC have been reported. The data samples used in the analysis correspond to an integrated luminosity of 35.9 fb^{-1} collected by the CMS detector in proton-proton collisions at $\sqrt{s} = 13 \text{ TeV}$.

The W^+W^- candidates are selected in events with large missing transverse momentum and exactly two, three, or four leptons. In the case of events with two leptons, different categories are defined according to the lepton pair flavor, $e\mu$, ee , or $\mu\mu$. The analysis has specific categories for gluon fusion production, vector boson fusion, and vector boson associated production, with up to two jets in the final state.

The probability of observing a signal at least as large as the one seen by combining all channels, under the background-only hypothesis, corresponds to an observed significance of 9.1 standard deviations for $m_H = 125.09$ GeV, to be compared with the expected value of 7.1 standard deviations. The observed global signal strength modifier is $\sigma/\sigma_{SM} = \mu = 1.28^{+0.18}_{-0.17} = 1.28 \pm 0.10$ (stat) ± 0.11 (syst) $^{+0.10}_{-0.07}$ (theo). Measurements of the signal strength modifiers associated with the main Higgs boson production mechanisms are also performed, as well as measurements of the Higgs boson couplings to fermions and vector bosons. The measured Higgs boson production and decay properties are found to be consistent, within their uncertainties, with the SM expectation.

Acknowledgments

We congratulate our colleagues in the CERN accelerator departments for the excellent performance of the LHC and thank the technical and administrative staffs at CERN and at other CMS institutes for their contributions to the success of the CMS effort. In addition, we gratefully acknowledge the computing centers and personnel of the Worldwide LHC Computing Grid for delivering so effectively the computing infrastructure essential to our analyses. Finally, we acknowledge the enduring support for the construction and operation of the LHC and the CMS detector provided by the following funding agencies: BMWFW and FWF (Austria); FNRS and FWO (Belgium); CNPq, CAPES, FAPERJ, FAPERGS, and FAPESP (Brazil); MES (Bulgaria); CERN; CAS, MoST, and NSFC (China); COLCIENCIAS (Colombia); MSES and CSF (Croatia); RPF (Cyprus); SENESCYT (Ecuador); MoER, ERC IUT, and ERDF (Estonia); Academy of Finland, MEC, and HIP (Finland); CEA and CNRS/IN2P3 (France); BMBF, DFG, and HGF (Germany); GSRT (Greece); NKFI (Hungary); DAE and DST (India); IPM (Iran); SFI (Ireland); INFN (Italy); MSIP and NRF (Republic of Korea); LAS (Lithuania); MOE and UM (Malaysia); BUAP, CINVESTAV, CONACYT, LNS, SEP, and UASLP-FAI (Mexico); MBIE (New Zealand); PAEC (Pakistan); MSHE and NSC (Poland); FCT (Portugal); JINR (Dubna); MON, RosAtom, RAS, RFBR, and NRC KI (Russia); MESTD (Serbia); SEIDI, CPAN, PCTI, and FEDER (Spain); Swiss Funding Agencies (Switzerland); MST (Taipei); ThEPCenter, IPST, STAR, and NSTDA (Thailand); TUBITAK and TAEK (Turkey); NASU and SFFR (Ukraine); STFC (United Kingdom); DOE and NSF (USA).

Individuals have received support from the Marie-Curie program and the European Research Council and Horizon 2020 Grant, contract No. 675440 (European Union); the Leventis Foundation; the A. P. Sloan Foundation; the Alexander von Humboldt Foundation; the Belgian Federal Science Policy Office; the Fonds pour la Formation à la Recherche dans l'Industrie et dans l'Agriculture (FRIA-Belgium); the Agentschap voor Innovatie door Wetenschap en Technologie (IWT-Belgium); the F.R.S.-FNRS and FWO (Belgium) under the "Excellence of Science - EOS" - be.h project n. 30820817; the Ministry of Education, Youth and Sports (MEYS) of the Czech Republic; the Lendület ("Momentum") Programme and the János Bolyai Research Scholarship of the Hungarian Academy of Sciences, the New National Excellence Program ÚNKP, the NKFI research grants 123842, 123959, 124845, 124850 and 125105 (Hungary); the Council of Science and Industrial Research, India; the HOMING PLUS program of the Foundation for Polish Science, cofinanced from European Union, Regional Development Fund, the

Mobility Plus program of the Ministry of Science and Higher Education, the National Science Center (Poland), contracts Harmonia 2014/14/M/ST2/00428, Opus 2014/13/B/ST2/02543, 2014/15/B/ST2/03998, and 2015/19/B/ST2/02861, Sonata-bis 2012/07/E/ST2/01406; the National Priorities Research Program by Qatar National Research Fund; the Programa Estatal de Fomento de la Investigación Científica y Técnica de Excelencia María de Maeztu, grant MDM-2015-0509 and the Programa Severo Ochoa del Principado de Asturias; the Thalís and Aristeia programs cofinanced by EU-ESF and the Greek NSRF; the Rachadapisek Sompot Fund for Postdoctoral Fellowship, Chulalongkorn University and the Chulalongkorn Academic into Its 2nd Century Project Advancement Project (Thailand); the Welch Foundation, contract C-1845; and the Weston Havens Foundation (USA).

References

- [1] F. Englert and R. Brout, “Broken symmetry and the mass of gauge vector mesons”, *Phys. Rev. Lett.* **13** (1964) 321, doi:10.1103/PhysRevLett.13.321.
- [2] P. W. Higgs, “Broken symmetries, massless particles and gauge fields”, *Phys. Lett.* **12** (1964) 132, doi:10.1016/0031-9163(64)91136-9.
- [3] P. W. Higgs, “Broken symmetries and the masses of gauge bosons”, *Phys. Rev. Lett.* **13** (1964) 508, doi:10.1103/PhysRevLett.13.508.
- [4] G. S. Guralnik, C. R. Hagen, and T. W. B. Kibble, “Global conservation laws and massless particles”, *Phys. Rev. Lett.* **13** (1964) 585, doi:10.1103/PhysRevLett.13.585.
- [5] P. W. Higgs, “Spontaneous symmetry breakdown without massless bosons”, *Phys. Rev.* **145** (1966) 1156, doi:10.1103/PhysRev.145.1156.
- [6] T. W. B. Kibble, “Symmetry breaking in non-Abelian gauge theories”, *Phys. Rev.* **155** (1967) 1554, doi:10.1103/PhysRev.155.1554.
- [7] ATLAS Collaboration, “Observation of a new particle in the search for the standard model Higgs boson with the ATLAS detector at the LHC”, *Phys. Lett. B* **716** (2012) 1, doi:10.1016/j.physletb.2012.08.020, arXiv:1207.7214.
- [8] CMS Collaboration, “Observation of a new boson at a mass of 125 GeV with the CMS experiment at the LHC”, *Phys. Lett. B* **716** (2012) 30, doi:10.1016/j.physletb.2012.08.021, arXiv:1207.7235.
- [9] CMS Collaboration, “Observation of a new boson with mass near 125 GeV in pp collisions at $\sqrt{s} = 7$ and 8 TeV”, *JHEP* **06** (2013) 081, doi:10.1007/JHEP06(2013)081, arXiv:1303.4571.
- [10] ATLAS Collaboration, “Measurements of the Higgs boson production and decay rates and coupling strengths using pp collision data at $\sqrt{s} = 7$ and 8 TeV in the ATLAS experiment”, *Eur. Phys. J. C* **76** (2016) 6, doi:10.1140/epjc/s10052-015-3769-y, arXiv:1507.04548.
- [11] ATLAS Collaboration, “Evidence for the spin-0 nature of the Higgs boson using ATLAS data”, *Phys. Lett. B* **726** (2013) 120, doi:10.1016/j.physletb.2013.08.026, arXiv:1307.1432.

- [12] CMS Collaboration, “Precise determination of the mass of the Higgs boson and tests of compatibility of its couplings with the standard model predictions using proton collisions at 7 and 8 TeV”, *Eur. Phys. J. C* **75** (2015) 212, doi:10.1140/epjc/s10052-015-3351-7, arXiv:1412.8662.
- [13] CMS Collaboration, “Constraints on the spin-parity and anomalous HVV couplings of the Higgs boson in proton collisions at 7 and 8 TeV”, *Phys. Rev. D* **92** (2015) 012004, doi:10.1103/PhysRevD.92.012004, arXiv:1411.3441.
- [14] ATLAS and CMS Collaborations, “Combined measurement of the Higgs boson mass in pp collisions at $\sqrt{s} = 7$ and 8 TeV with the ATLAS and CMS experiments”, *Phys. Rev. Lett.* **114** (2015) 191803, doi:10.1103/PhysRevLett.114.191803, arXiv:1503.07589.
- [15] ATLAS and CMS Collaborations, “Measurements of the Higgs boson production and decay rates and constraints on its couplings from a combined ATLAS and CMS analysis of the LHC pp collision data at $\sqrt{s} = 7$ and 8 TeV”, *JHEP* **08** (2016) 045, doi:10.1007/JHEP08(2016)045, arXiv:1606.02266.
- [16] ATLAS Collaboration, “Observation and measurement of Higgs boson decays to WW^* with the ATLAS detector”, *Phys. Rev. D* **92** (2015) 012006, doi:10.1103/PhysRevD.92.012006, arXiv:1412.2641.
- [17] ATLAS Collaboration, “Study of $(W/Z)H$ production and Higgs boson couplings using $H \rightarrow WW^*$ decays with the ATLAS detector”, *JHEP* **08** (2015) 137, doi:10.1007/JHEP08(2015)137, arXiv:1506.06641.
- [18] CMS Collaboration, “Measurement of Higgs boson production and properties in the WW decay channel with leptonic final states”, *JHEP* **01** (2014) 096, doi:10.1007/JHEP01(2014)096, arXiv:1312.1129.
- [19] ATLAS Collaboration, “Constraints on the off-shell Higgs boson signal strength in the high-mass ZZ and WW final states with the ATLAS detector”, *Eur. Phys. J. C* **75** (2015) 335, doi:10.1140/epjc/s10052-015-3542-2, arXiv:1503.01060.
- [20] CMS Collaboration, “Search for Higgs boson off-shell production in proton-proton collisions at 7 and 8 TeV and derivation of constraints on its total decay width”, *JHEP* **09** (2016) 051, doi:10.1007/JHEP09(2016)051, arXiv:1605.02329.
- [21] ATLAS Collaboration, “Measurement of fiducial differential cross sections of gluon-fusion production of Higgs bosons decaying to $WW^* \rightarrow e\nu\mu\nu$ with the ATLAS detector at $\sqrt{s} = 8$ TeV”, *JHEP* **08** (2016) 104, doi:10.1007/JHEP08(2016)104, arXiv:1604.02997.
- [22] CMS Collaboration, “Measurement of the transverse momentum spectrum of the Higgs boson produced in pp collisions at $\sqrt{s} = 8$ TeV using $H \rightarrow WW$ decays”, *JHEP* **03** (2017) 032, doi:10.1007/JHEP03(2017)032, arXiv:1606.01522.
- [23] ATLAS Collaboration, “Measurements of gluon-gluon fusion and vector-boson fusion Higgs boson production cross-sections in the $H \rightarrow WW^* \rightarrow e\nu\mu\nu$ decay channel in pp collisions at $\sqrt{s} = 13$ TeV with the ATLAS detector”, (2018). arXiv:1808.09054.
- [24] CMS Collaboration, “The CMS experiment at the CERN LHC”, *JINST* **3** (2008) S08004, doi:10.1088/1748-0231/3/08/S08004.

-
- [25] P. Nason, “A new method for combining NLO QCD with shower Monte Carlo algorithms”, *JHEP* **11** (2004) 040, doi:10.1088/1126-6708/2004/11/040, arXiv:hep-ph/0409146.
- [26] S. Frixione, P. Nason, and C. Oleari, “Matching NLO QCD computations with parton shower simulations: the POWHEG method”, *JHEP* **11** (2007) 070, doi:10.1088/1126-6708/2007/11/070, arXiv:0709.2092.
- [27] S. Alioli, P. Nason, C. Oleari, and E. Re, “A general framework for implementing NLO calculations in shower Monte Carlo programs: the POWHEG BOX”, *JHEP* **06** (2010) 043, doi:10.1007/JHEP06(2010)043, arXiv:1002.2581.
- [28] E. Bagnaschi, G. Degrossi, P. Slavich, and A. Vicini, “Higgs production via gluon fusion in the POWHEG approach in the SM and in the MSSM”, *JHEP* **02** (2012) 088, doi:10.1007/JHEP02(2012)088, arXiv:1111.2854.
- [29] K. Hamilton, P. Nason, E. Re, and G. Zanderighi, “NNLOPS simulation of Higgs boson production”, *JHEP* **10** (2013) 222, doi:10.1007/JHEP10(2013)222, arXiv:1309.0017.
- [30] G. Luisoni, P. Nason, C. Oleari, and F. Tramontano, “ $HW^\pm/HZ + 0$ and 1 jet at NLO with the POWHEG BOX interfaced to GoSam and their merging within MiNLO”, *JHEP* **10** (2013) 083, doi:10.1007/JHEP10(2013)083, arXiv:1306.2542.
- [31] J. Alwall et al., “The automated computation of tree-level and next-to-leading order differential cross sections, and their matching to parton shower simulations”, *JHEP* **07** (2014) 079, doi:10.1007/JHEP07(2014)079, arXiv:1405.0301.
- [32] S. Alioli, P. Nason, C. Oleari, and E. Re, “NLO Higgs boson production via gluon fusion matched with shower in POWHEG”, *JHEP* **04** (2009) 002, doi:10.1088/1126-6708/2009/04/002, arXiv:0812.0578.
- [33] P. Nason and C. Oleari, “NLO Higgs boson production via vector-boson fusion matched with shower in POWHEG”, *JHEP* **02** (2010) 037, doi:10.1007/JHEP02(2010)037, arXiv:0911.5299.
- [34] Y. Gao et al., “Spin determination of single-produced resonances at hadron colliders”, *Phys. Rev. D* **81** (2010) 075022, doi:10.1103/PhysRevD.81.075022, arXiv:1001.3396.
- [35] S. Bolognesi et al., “On the spin and parity of a single-produced resonance at the LHC”, *Phys. Rev. D* **86** (2012) 095031, doi:10.1103/PhysRevD.86.095031, arXiv:1208.4018.
- [36] T. Sjöstrand, S. Mrenna, and P. Z. Skands, “A brief introduction to PYTHIA 8.1”, *Comput. Phys. Commun.* **178** (2008) 852, doi:10.1016/j.cpc.2008.01.036, arXiv:0710.3820.
- [37] LHC Higgs Cross Section Working Group Collaboration, “Handbook of LHC Higgs cross sections: 4. Deciphering the nature of the Higgs sector”, (2016). arXiv:1610.07922.
- [38] LHC Higgs Cross Section Working Group Collaboration, “Handbook of LHC Higgs cross sections: 3. Higgs properties”, (2013). arXiv:1307.1347.

- [39] T. Melia, P. Nason, R. Röntsch, and G. Zanderighi, “ W^+W^- , WZ and ZZ production in the POWHEG BOX”, *JHEP* **11** (2011) 078, doi:10.1007/JHEP11(2011)078, arXiv:1107.5051.
- [40] J. M. Campbell, R. K. Ellis, and C. Williams, “Bounding the Higgs width at the LHC: Complementary results from $H \rightarrow WW$ ”, *Phys. Rev. D* **89** (2014) 053011, doi:10.1103/PhysRevD.89.053011, arXiv:1312.1628.
- [41] P. Meade, H. Ramani, and M. Zeng, “Transverse momentum resummation effects in W^+W^- measurements”, *Phys. Rev. D* **90** (2014) 114006, doi:10.1103/PhysRevD.90.114006, arXiv:1407.4481.
- [42] P. Jaiswal and T. Okui, “Explanation of the WW excess at the LHC by jet-veto resummation”, *Phys. Rev. D* **90** (2014) 073009, doi:10.1103/PhysRevD.90.073009, arXiv:1407.4537.
- [43] F. Caola, K. Melnikov, R. Röntsch, and L. Tancredi, “QCD corrections to W^+W^- production through gluon fusion”, *Phys. Lett. B* **754** (2016) 275, doi:10.1016/j.physletb.2016.01.046, arXiv:1511.08617.
- [44] P. Kant et al., “HatHor for single top-quark production: Updated predictions and uncertainty estimates for single top-quark production in hadronic collisions”, *Comput. Phys. Commun.* **191** (2015) 74, doi:10.1016/j.cpc.2015.02.001, arXiv:1406.4403.
- [45] M. Czakon and A. Mitov, “Top++: a program for the calculation of the top-pair cross-section at hadron colliders”, *Comput. Phys. Commun.* **185** (2014) 2930, doi:10.1016/j.cpc.2014.06.021, arXiv:1112.5675.
- [46] R. Frederix and S. Frixione, “Merging meets matching in MC@NLO”, *JHEP* **12** (2012) 061, doi:10.1007/JHEP12(2012)061, arXiv:1209.6215.
- [47] NNPDF Collaboration, “Parton distributions with QED corrections”, *Nucl. Phys. B* **877** (2013) 290, doi:10.1016/j.nuclphysb.2013.10.010, arXiv:1308.0598.
- [48] NNPDF Collaboration, “Unbiased global determination of parton distributions and their uncertainties at NNLO and at LO”, *Nucl. Phys. B* **855** (2012) 153, doi:10.1016/j.nuclphysb.2011.09.024, arXiv:1107.2652.
- [49] CMS Collaboration, “Event generator tunes obtained from underlying event and multiparton scattering measurements”, *Eur. Phys. J. C* **76** (2016) 155, doi:10.1140/epjc/s10052-016-3988-x, arXiv:1512.00815.
- [50] P. Richardson and A. Wilcock, “Monte Carlo simulation of hard radiation in decays in beyond the standard model physics in Herwig++”, *Eur. Phys. J. C* **74** (2014) 2713, doi:10.1140/epjc/s10052-014-2713-x, arXiv:1303.4563.
- [51] J. Bellm et al., “Herwig++ 2.7 release note”, (2013). arXiv:1310.6877.
- [52] GEANT4 Collaboration, “GEANT4—a simulation toolkit”, *Nucl. Instrum. Meth. A* **506** (2003) 250, doi:10.1016/S0168-9002(03)01368-8.
- [53] CMS Collaboration, “Particle-flow reconstruction and global event description with the CMS detector”, *JINST* **12** (2017) P10003, doi:10.1088/1748-0221/12/10/P10003, arXiv:1706.04965.

- [54] M. Cacciari, G. P. Salam, and G. Soyez, “The anti- k_T jet clustering algorithm”, *JHEP* **04** (2008) 063, doi:10.1088/1126-6708/2008/04/063, arXiv:0802.1189.
- [55] M. Cacciari, G. P. Salam, and G. Soyez, “FastJet user manual”, *Eur. Phys. J. C* **72** (2012) 1896, doi:10.1140/epjc/s10052-012-1896-2, arXiv:1111.6097.
- [56] CMS Collaboration, “Performance of electron reconstruction and selection with the CMS detector in proton-proton collisions at $\sqrt{s} = 8$ TeV”, *JINST* **10** (2015) P06005, doi:10.1088/1748-0221/10/06/P06005, arXiv:1502.02701.
- [57] M. Cacciari and G. P. Salam, “Pileup subtraction using jet areas”, *Phys. Lett. B* **659** (2008) 119, doi:10.1016/j.physletb.2007.09.077, arXiv:0707.1378.
- [58] CMS Collaboration, “Determination of jet energy calibration and transverse momentum resolution in CMS”, *JINST* **6** (2011) P11002, doi:10.1088/1748-0221/6/11/P11002, arXiv:1107.4277.
- [59] CMS Collaboration, “Identification of heavy-flavour jets with the CMS detector in pp collisions at 13 TeV”, *JINST* **13** (2018) P05011, doi:10.1088/1748-0221/13/05/P05011, arXiv:1712.07158.
- [60] CMS Collaboration, “Measurement of differential cross sections for top quark pair production using the lepton+jets final state in proton-proton collisions at 13 TeV”, *Phys. Rev. D* **95** (2017) 092001, doi:10.1103/PhysRevD.95.092001, arXiv:1610.04191.
- [61] G. Passarino, “Higgs CAT”, *Eur. Phys. J. C* **74** (2014) 2866, doi:10.1140/epjc/s10052-014-2866-7, arXiv:1312.2397.
- [62] ATLAS and CMS Collaborations, LHC Higgs Combination Group, “Procedure for the LHC Higgs boson search combination in Summer 2011”, Technical Report ATL-PHYS-PUB 2011-11, CMS NOTE 2011/005, CERN, 2011.
- [63] CMS Collaboration, “CMS luminosity measurements for the 2016 data taking period”, CMS Physics Analysis Summary CMS-PAS-LUM-17-001, 2017.
- [64] CMS Collaboration, “The CMS trigger system”, *JINST* **12** (2017) P01020, doi:10.1088/1748-0221/12/01/P01020, arXiv:1609.02366.
- [65] CMS Collaboration, “Performance of CMS muon reconstruction in pp collision events at $\sqrt{s} = 7$ TeV”, *JINST* **7** (2012) P10002, doi:10.1088/1748-0221/7/10/P10002, arXiv:1206.4071.
- [66] CMS Collaboration, “Jet energy scale and resolution in the CMS experiment in pp collisions at 8 TeV”, *JINST* **12** (2017) P02014, doi:10.1088/1748-0221/12/02/P02014, arXiv:1607.03663.
- [67] J. Butterworth et al., “PDF4LHC recommendations for LHC Run II”, *J. Phys. G* **43** (2016) 023001, doi:10.1088/0954-3899/43/2/023001, arXiv:1510.03865.
- [68] G. Cowan, K. Cranmer, E. Gross, and O. Vitells, “Asymptotic formulae for likelihood-based tests of new physics”, *Eur. Phys. J. C* **71** (2011) 1, doi:10.1140/epjc/s10052-011-1554-0, arXiv:1007.1727.

A The CMS Collaboration

Yerevan Physics Institute, Yerevan, Armenia

A.M. Sirunyan, A. Tumasyan

Institut für Hochenergiephysik, Wien, Austria

W. Adam, F. Ambrogio, E. Asilar, T. Bergauer, J. Brandstetter, M. Dragicevic, J. Erö, A. Escalante Del Valle, M. Flechl, R. Frühwirth¹, V.M. Ghete, J. Hrubec, M. Jeitler¹, N. Krammer, I. Krätschmer, D. Liko, T. Madlener, I. Mikulec, N. Rad, H. Rohringer, J. Schieck¹, R. Schöfbeck, M. Spanring, D. Spitzbart, A. Taurok, W. Waltenberger, J. Wittmann, C.-E. Wulz¹, M. Zarucki

Institute for Nuclear Problems, Minsk, Belarus

V. Chekhovsky, V. Mossolov, J. Suarez Gonzalez

Universiteit Antwerpen, Antwerpen, Belgium

E.A. De Wolf, D. Di Croce, X. Janssen, J. Lauwers, M. Pieters, M. Van De Klundert, H. Van Haevermaet, P. Van Mechelen, N. Van Remortel

Vrije Universiteit Brussel, Brussel, Belgium

S. Abu Zeid, F. Blekman, J. D'Hondt, I. De Bruyn, J. De Clercq, K. Deroover, G. Flouris, D. Lontkovskyi, S. Lowette, I. Marchesini, S. Moortgat, L. Moreels, Q. Python, K. Skovpen, S. Tavernier, W. Van Doninck, P. Van Mulders, I. Van Parijs

Université Libre de Bruxelles, Bruxelles, Belgium

D. Beghin, B. Bilin, H. Brun, B. Clerboux, G. De Lentdecker, H. Delannoy, B. Dorney, G. Fasanella, L. Favart, R. Goldouzian, A. Grebenyuk, A.K. Kalsi, T. Lenzi, J. Luetic, N. Postiau, E. Starling, L. Thomas, C. Vander Velde, P. Vanlaer, D. Vannerom, Q. Wang

Ghent University, Ghent, Belgium

T. Cornelis, D. Dobur, A. Fagot, M. Gul, I. Khvastunov², D. Poyraz, C. Roskas, D. Trocino, M. Tytgat, W. Verbeke, B. Vermassen, M. Vit, N. Zaganidis

Université Catholique de Louvain, Louvain-la-Neuve, Belgium

H. Bakhshiansohi, O. Bondu, S. Brochet, G. Bruno, C. Caputo, P. David, C. Delaere, M. Delcourt, B. Francois, A. Giammanco, G. Krintiras, V. Lemaitre, A. Magitteri, A. Mertens, M. Musich, K. Piotrkowski, A. Saggio, M. Vidal Marono, S. Wertz, J. Zobec

Centro Brasileiro de Pesquisas Físicas, Rio de Janeiro, Brazil

F.L. Alves, G.A. Alves, L. Brito, M. Correa Martins Junior, G. Correia Silva, C. Hensel, A. Moraes, M.E. Pol, P. Rebello Teles

Universidade do Estado do Rio de Janeiro, Rio de Janeiro, Brazil

E. Belchior Batista Das Chagas, W. Carvalho, J. Chinellato³, E. Coelho, E.M. Da Costa, G.G. Da Silveira⁴, D. De Jesus Damiao, C. De Oliveira Martins, S. Fonseca De Souza, H. Malbouisson, D. Matos Figueiredo, M. Melo De Almeida, C. Mora Herrera, L. Mundim, H. Nogima, W.L. Prado Da Silva, L.J. Sanchez Rosas, A. Santoro, A. Sznajder, M. Thiel, E.J. Tonelli Manganote³, F. Torres Da Silva De Araujo, A. Vilela Pereira

Universidade Estadual Paulista ^a, Universidade Federal do ABC ^b, São Paulo, Brazil

S. Ahuja^a, C.A. Bernardes^a, L. Calligaris^a, T.R. Fernandez Perez Tomei^a, E.M. Gregores^b, P.G. Mercadante^b, S.F. Novaes^a, SandraS. Padula^a, D. Romero Abad^b

Institute for Nuclear Research and Nuclear Energy, Bulgarian Academy of Sciences, Sofia,

Bulgaria

A. Aleksandrov, R. Hadjiiska, P. Iaydjiev, A. Marinov, M. Misheva, M. Rodozov, M. Shopova, G. Sultanov

University of Sofia, Sofia, Bulgaria

A. Dimitrov, L. Litov, B. Pavlov, P. Petkov

Beihang University, Beijing, China

W. Fang⁵, X. Gao⁵, L. Yuan

Institute of High Energy Physics, Beijing, China

M. Ahmad, J.G. Bian, G.M. Chen, H.S. Chen, M. Chen, Y. Chen, C.H. Jiang, D. Leggat, H. Liao, Z. Liu, F. Romeo, S.M. Shaheen⁶, A. Spiezia, J. Tao, C. Wang, Z. Wang, E. Yazgan, H. Zhang, J. Zhao

State Key Laboratory of Nuclear Physics and Technology, Peking University, Beijing, China

Y. Ban, G. Chen, A. Levin, J. Li, L. Li, Q. Li, Y. Mao, S.J. Qian, D. Wang, Z. Xu

Tsinghua University, Beijing, China

Y. Wang

Universidad de Los Andes, Bogota, Colombia

C. Avila, A. Cabrera, C.A. Carrillo Montoya, L.F. Chaparro Sierra, C. Florez, C.F. González Hernández, M.A. Segura Delgado

University of Split, Faculty of Electrical Engineering, Mechanical Engineering and Naval Architecture, Split, Croatia

B. Courbon, N. Godinovic, D. Lelas, I. Puljak, T. Sculac

University of Split, Faculty of Science, Split, Croatia

Z. Antunovic, M. Kovac

Institute Rudjer Boskovic, Zagreb, Croatia

V. Brigljevic, D. Ferencek, K. Kadija, B. Mesic, A. Starodumov⁷, T. Susa

University of Cyprus, Nicosia, Cyprus

M.W. Ather, A. Attikis, M. Kolosova, G. Mavromanolakis, J. Mousa, C. Nicolaou, F. Ptochos, P.A. Razis, H. Rykaczewski

Charles University, Prague, Czech Republic

M. Finger⁸, M. Finger Jr.⁸

Escuela Politecnica Nacional, Quito, Ecuador

E. Ayala

Universidad San Francisco de Quito, Quito, Ecuador

E. Carrera Jarrin

Academy of Scientific Research and Technology of the Arab Republic of Egypt, Egyptian Network of High Energy Physics, Cairo, Egypt

H. Abdalla⁹, A.A. Abdelalim^{10,11}, A. Mohamed¹¹

National Institute of Chemical Physics and Biophysics, Tallinn, Estonia

S. Bhowmik, A. Carvalho Antunes De Oliveira, R.K. Dewanjee, K. Ehataht, M. Kadastik, M. Raidal, C. Veelken

Department of Physics, University of Helsinki, Helsinki, Finland

P. Eerola, H. Kirschenmann, J. Pekkanen, M. Voutilainen

Helsinki Institute of Physics, Helsinki, Finland

J. Havukainen, J.K. Heikkilä, T. Järvinen, V. Karimäki, R. Kinnunen, T. Lampén, K. Lassila-Perini, S. Laurila, S. Lehti, T. Lindén, P. Luukka, T. Mäenpää, H. Siikonen, E. Tuominen, J. Tuominiemi

Lappeenranta University of Technology, Lappeenranta, Finland

T. Tuuva

IRFU, CEA, Université Paris-Saclay, Gif-sur-Yvette, France

M. Besancon, F. Couderc, M. Dejardin, D. Denegri, J.L. Faure, F. Ferri, S. Ganjour, A. Givernaud, P. Gras, G. Hamel de Monchenault, P. Jarry, C. Leloup, E. Locci, J. Malcles, G. Negro, J. Rander, A. Rosowsky, M.Ö. Sahin, M. Titov

Laboratoire Leprince-Ringuet, Ecole polytechnique, CNRS/IN2P3, Université Paris-Saclay, Palaiseau, France

A. Abdulsalam¹², C. Amendola, I. Antropov, F. Beaudette, P. Busson, C. Charlot, R. Granier de Cassagnac, I. Kucher, A. Lobanov, J. Martin Blanco, M. Nguyen, C. Ochando, G. Ortona, P. Pigard, R. Salerno, J.B. Sauvan, Y. Sirois, A.G. Stahl Leiton, A. Zabi, A. Zghiche

Université de Strasbourg, CNRS, IPHC UMR 7178, Strasbourg, France

J.-L. Agram¹³, J. Andrea, D. Bloch, J.-M. Brom, E.C. Chabert, V. Cherepanov, C. Collard, E. Conte¹³, J.-C. Fontaine¹³, D. Gelé, U. Goerlach, M. Jansová, A.-C. Le Bihan, N. Tonon, P. Van Hove

Centre de Calcul de l'Institut National de Physique Nucleaire et de Physique des Particules, CNRS/IN2P3, Villeurbanne, France

S. Gadrat

Université de Lyon, Université Claude Bernard Lyon 1, CNRS-IN2P3, Institut de Physique Nucléaire de Lyon, Villeurbanne, France

S. Beauceron, C. Bernet, G. Boudoul, N. Chanon, R. Chierici, D. Contardo, P. Depasse, H. El Mamouni, J. Fay, L. Finco, S. Gascon, M. Gouzevitch, G. Grenier, B. Ille, F. Lagarde, I.B. Laktineh, H. Lattaud, M. Lethuillier, L. Mirabito, A.L. Pequegnot, S. Perries, A. Popov¹⁴, V. Sordini, M. Vander Donckt, S. Viret, S. Zhang

Georgian Technical University, Tbilisi, Georgia

A. Khvedelidze⁸

Tbilisi State University, Tbilisi, Georgia

Z. Tsamalaidze⁸

RWTH Aachen University, I. Physikalisches Institut, Aachen, Germany

C. Autermann, L. Feld, M.K. Kiesel, K. Klein, M. Lipinski, M. Preuten, M.P. Rauch, C. Schomakers, J. Schulz, M. Teroerde, B. Wittmer, V. Zhukov¹⁴

RWTH Aachen University, III. Physikalisches Institut A, Aachen, Germany

A. Albert, D. Duchardt, M. Endres, M. Erdmann, T. Esch, R. Fischer, S. Ghosh, A. Güth, T. Hebbeker, C. Heidemann, K. Hoepfner, H. Keller, S. Knutzen, L. Mastrolorenzo, M. Merschmeyer, A. Meyer, P. Millet, S. Mukherjee, T. Pook, M. Radziej, H. Reithler, M. Rieger, F. Scheuch, A. Schmidt, D. Teyssier

RWTH Aachen University, III. Physikalisches Institut B, Aachen, Germany

G. Flügge, O. Hlushchenko, T. Kress, A. Künsken, T. Müller, A. Nehr Korn, A. Nowack, C. Pistone, O. Pooth, D. Roy, H. Sert, A. Stahl¹⁵

Deutsches Elektronen-Synchrotron, Hamburg, Germany

M. Aldaya Martin, T. Arndt, C. Asawatangtrakuldee, I. Babounikau, K. Beernaert, O. Behnke, U. Behrens, A. Bermúdez Martínez, D. Bertsche, A.A. Bin Anuar, K. Borras¹⁶, V. Botta, A. Campbell, P. Connor, C. Contreras-Campana, F. Costanza, V. Danilov, A. De Wit, M.M. Defranchis, C. Diez Pardos, D. Domínguez Damiani, G. Eckerlin, T. Eichhorn, A. Elwood, E. Eren, E. Gallo¹⁷, A. Geiser, J.M. Grados Luyando, A. Grohsjean, P. Gunnellini, M. Guthoff, M. Haranko, A. Harb, J. Hauk, H. Jung, M. Kasemann, J. Keaveney, C. Kleinwort, J. Knolle, D. Krücker, W. Lange, A. Lelek, T. Lenz, K. Lipka, W. Lohmann¹⁸, R. Mankel, I.-A. Melzer-Pellmann, A.B. Meyer, M. Meyer, M. Missiroli, G. Mittag, J. Mnich, V. Myronenko, S.K. Pflitsch, D. Pitzl, A. Raspereza, M. Savitskyi, P. Saxena, P. Schütze, C. Schwanenberger, R. Shevchenko, A. Singh, H. Tholen, O. Turkot, A. Vagnerini, G.P. Van Onsem, R. Walsh, Y. Wen, K. Wichmann, C. Wissing, O. Zenaiev

University of Hamburg, Hamburg, Germany

R. Aggleton, S. Bein, L. Benato, A. Benecke, V. Blobel, M. Centis Vignali, T. Dreyer, E. Garutti, D. Gonzalez, J. Haller, A. Hinzmann, A. Karavdina, G. Kasieczka, R. Klanner, R. Kogler, N. Kovalchuk, S. Kurz, V. Kutzner, J. Lange, D. Marconi, J. Multhaup, M. Niedziela, D. Nowatschin, A. Perieanu, A. Reimers, O. Rieger, C. Scharf, P. Schleper, S. Schumann, J. Schwandt, J. Sonneveld, H. Stadie, G. Steinbrück, F.M. Stober, M. Stöver, D. Troendle, A. Vanhoefer, B. Vormwald

Karlsruher Institut fuer Technology

M. Akbiyik, C. Barth, M. Baselga, S. Baur, E. Butz, R. Caspart, T. Chwalek, F. Colombo, W. De Boer, A. Dierlamm, K. El Morabit, N. Faltermann, B. Freund, M. Giffels, M.A. Harrendorf, F. Hartmann¹⁵, S.M. Heindl, U. Husemann, F. Kassel¹⁵, I. Katkov¹⁴, S. Kudella, H. Mildner, S. Mitra, M.U. Mozer, Th. Müller, M. Plagge, G. Quast, K. Rabbertz, M. Schröder, I. Shvetsov, G. Sieber, H.J. Simonis, R. Ulrich, S. Wayand, M. Weber, T. Weiler, S. Williamson, C. Wöhrmann, R. Wolf

Institute of Nuclear and Particle Physics (INPP), NCSR Demokritos, Aghia Paraskevi, Greece

G. Anagnostou, G. Daskalakis, T. Gerasis, A. Kyriakis, D. Loukas, G. Paspalaki, I. Topsis-Giotis

National and Kapodistrian University of Athens, Athens, Greece

G. Karathanasis, S. Kesisoglou, P. Kontaxakis, A. Panagiotou, I. Papavergou, N. Saoulidou, E. Tziaferi, K. Vellidis

National Technical University of Athens, Athens, Greece

K. Kousouris, I. Papakrivopoulos, G. Tsipolitis

University of Ioánnina, Ioánnina, Greece

I. Evangelou, C. Foudas, P. Giannelis, P. Katsoulis, P. Kokkas, S. Mallios, N. Manthos, I. Papadopoulos, E. Paradas, J. Strologas, F.A. Triantis, D. Tsitsonis

MTA-ELTE Lendület CMS Particle and Nuclear Physics Group, Eötvös Loránd University, Budapest, Hungary

M. Bartók¹⁹, M. Csanad, N. Filipovic, P. Major, M.I. Nagy, G. Pasztor, O. Surányi, G.I. Veres

Wigner Research Centre for Physics, Budapest, Hungary

G. Bencze, C. Hajdu, D. Horvath²⁰, Á. Hunyadi, F. Sikler, T.Á. Vámi, V. Veszpremi, G. Vesztergombi[†]

Institute of Nuclear Research ATOMKI, Debrecen, Hungary

N. Beni, S. Czellar, J. Karancsi²¹, A. Makovec, J. Molnar, Z. Szillasi

Institute of Physics, University of Debrecen, Debrecen, Hungary

P. Raics, Z.L. Trocsanyi, B. Ujvari

Indian Institute of Science (IISc), Bangalore, India

S. Choudhury, J.R. Komaragiri, P.C. Tiwari

National Institute of Science Education and Research, HBNI, Bhubaneswar, India

S. Bahinipati²², C. Kar, P. Mal, K. Mandal, A. Nayak²³, D.K. Sahoo²², S.K. Swain

Panjab University, Chandigarh, India

S. Bansal, S.B. Beri, V. Bhatnagar, S. Chauhan, R. Chawla, N. Dhingra, R. Gupta, A. Kaur, A. Kaur, M. Kaur, S. Kaur, R. Kumar, P. Kumari, M. Lohan, A. Mehta, K. Sandeep, S. Sharma, J.B. Singh, G. Walia

University of Delhi, Delhi, India

A. Bhardwaj, B.C. Choudhary, R.B. Garg, M. Gola, S. Keshri, Ashok Kumar, S. Malhotra, M. Naimuddin, P. Priyanka, K. Ranjan, Aashaq Shah, R. Sharma

Saha Institute of Nuclear Physics, HBNI, Kolkata, India

R. Bhardwaj²⁴, M. Bharti, R. Bhattacharya, S. Bhattacharya, U. Bhawandeep²⁴, D. Bhowmik, S. Dey, S. Dutt²⁴, S. Dutta, S. Ghosh, K. Mondal, S. Nandan, A. Purohit, P.K. Rout, A. Roy, S. Roy Chowdhury, G. Saha, S. Sarkar, M. Sharan, B. Singh, S. Thakur²⁴

Indian Institute of Technology Madras, Madras, India

P.K. Behera

Bhabha Atomic Research Centre, Mumbai, India

R. Chudasama, D. Dutta, V. Jha, V. Kumar, P.K. Netrakanti, L.M. Pant, P. Shukla

Tata Institute of Fundamental Research-A, Mumbai, India

T. Aziz, M.A. Bhat, S. Dugad, G.B. Mohanty, N. Sur, B. Sutar, RavindraKumar Verma

Tata Institute of Fundamental Research-B, Mumbai, India

S. Banerjee, S. Bhattacharya, S. Chatterjee, P. Das, M. Guchait, Sa. Jain, S. Karmakar, S. Kumar, M. Maity²⁵, G. Majumder, K. Mazumdar, N. Sahoo, T. Sarkar²⁵

Indian Institute of Science Education and Research (IISER), Pune, India

S. Chauhan, S. Dube, V. Hegde, A. Kapoor, K. Kothekar, S. Pandey, A. Rane, S. Sharma

Institute for Research in Fundamental Sciences (IPM), Tehran, Iran

S. Chenarani²⁶, E. Eskandari Tadavani, S.M. Etesami²⁶, M. Khakzad, M. Mohammadi Najafabadi, M. Naseri, F. Rezaei Hosseinabadi, B. Safarzadeh²⁷, M. Zeinali

University College Dublin, Dublin, Ireland

M. Felcini, M. Grunewald

INFN Sezione di Bari ^a, Università di Bari ^b, Politecnico di Bari ^c, Bari, Italy

M. Abbrescia^{a,b}, C. Calabria^{a,b}, A. Colaleo^a, D. Creanza^{a,c}, L. Cristella^{a,b}, N. De Filippis^{a,c}, M. De Palma^{a,b}, A. Di Florio^{a,b}, F. Errico^{a,b}, L. Fiore^a, A. Gelmi^{a,b}, G. Iaselli^{a,c}, M. Ince^{a,b}, S. Lezki^{a,b}, G. Maggi^{a,c}, M. Maggi^a, G. Miniello^{a,b}, S. My^{a,b}, S. Nuzzo^{a,b}, A. Pompili^{a,b},

G. Pugliese^{a,c}, R. Radogna^a, A. Ranieri^a, G. Selvaggi^{a,b}, A. Sharma^a, L. Silvestris^a, R. Venditti^a, P. Verwilligen^a, G. Zito^a

INFN Sezione di Bologna ^a, Università di Bologna ^b, Bologna, Italy

G. Abbiendi^a, C. Battilana^{a,b}, D. Bonacorsi^{a,b}, L. Borgonovi^{a,b}, S. Braibant-Giacomelli^{a,b}, R. Campanini^{a,b}, P. Capiluppi^{a,b}, A. Castro^{a,b}, F.R. Cavallo^a, S.S. Chhibra^{a,b}, C. Ciocca^a, G. Codispoti^{a,b}, M. Cuffiani^{a,b}, G.M. Dallavalle^a, F. Fabbri^a, A. Fanfani^{a,b}, P. Giacomelli^a, C. Grandi^a, L. Guiducci^{a,b}, F. Iemmi^{a,b}, S. Marcellini^a, G. Masetti^a, A. Montanari^a, F.L. Navarria^{a,b}, A. Perrotta^a, F. Primavera^{a,b,15}, A.M. Rossi^{a,b}, T. Rovelli^{a,b}, G.P. Siroli^{a,b}, N. Tosi^a

INFN Sezione di Catania ^a, Università di Catania ^b, Catania, Italy

S. Albergo^{a,b}, A. Di Mattia^a, R. Potenza^{a,b}, A. Tricomi^{a,b}, C. Tuve^{a,b}

INFN Sezione di Firenze ^a, Università di Firenze ^b, Firenze, Italy

G. Barbagli^a, K. Chatterjee^{a,b}, V. Ciulli^{a,b}, C. Civinini^a, R. D'Alessandro^{a,b}, E. Focardi^{a,b}, G. Latino, P. Lenzi^{a,b}, M. Meschini^a, S. Paoletti^a, L. Russo^{a,28}, G. Sguazzoni^a, D. Strom^a, L. Viliani^a

INFN Laboratori Nazionali di Frascati, Frascati, Italy

L. Benussi, S. Bianco, F. Fabbri, D. Piccolo

INFN Sezione di Genova ^a, Università di Genova ^b, Genova, Italy

F. Ferro^a, F. Ravera^{a,b}, E. Robutti^a, S. Tosi^{a,b}

INFN Sezione di Milano-Bicocca ^a, Università di Milano-Bicocca ^b, Milano, Italy

A. Benaglia^a, A. Beschi^b, L. Brianza^{a,b}, F. Brivio^{a,b}, V. Ciriolo^{a,b,15}, S. Di Guida^{a,d,15}, M.E. Dinardo^{a,b}, S. Fiorendi^{a,b}, S. Gennai^a, A. Ghezzi^{a,b}, P. Govoni^{a,b}, M. Malberti^{a,b}, S. Malvezzi^a, A. Massironi^{a,b}, D. Menasce^a, L. Moroni^a, M. Paganoni^{a,b}, D. Pedrini^a, S. Ragazzi^{a,b}, T. Tabarelli de Fatis^{a,b}, D. Zuolo

INFN Sezione di Napoli ^a, Università di Napoli 'Federico II' ^b, Napoli, Italy, Università della Basilicata ^c, Potenza, Italy, Università G. Marconi ^d, Roma, Italy

S. Buontempo^a, N. Cavallo^{a,c}, A. Di Crescenzo^{a,b}, F. Fabozzi^{a,c}, F. Fienga^a, G. Galati^a, A.O.M. Iorio^{a,b}, W.A. Khan^a, L. Lista^a, S. Meola^{a,d,15}, P. Paolucci^{a,15}, C. Sciacca^{a,b}, E. Voevodina^{a,b}

INFN Sezione di Padova ^a, Università di Padova ^b, Padova, Italy, Università di Trento ^c, Trento, Italy

P. Azzi^a, N. Bacchetta^a, D. Bisello^{a,b}, A. Boletti^{a,b}, A. Bragagnolo, R. Carlin^{a,b}, P. Checchia^a, M. Dall'Osso^{a,b}, P. De Castro Manzano^a, T. Dorigo^a, U. Dosselli^a, F. Gasparini^{a,b}, U. Gasparini^{a,b}, S.Y. Hoh, S. Lacaprara^a, P. Lujan, M. Margoni^{a,b}, A.T. Meneguzzo^{a,b}, J. Pazzini^{a,b}, N. Pozzobon^{a,b}, P. Ronchese^{a,b}, R. Rossin^{a,b}, F. Simonetto^{a,b}, A. Tiko, E. Torassa^a, S. Ventura^a, M. Zanetti^{a,b}, P. Zotto^{a,b}

INFN Sezione di Pavia ^a, Università di Pavia ^b, Pavia, Italy

A. Braghieri^a, A. Magnani^a, P. Montagna^{a,b}, S.P. Ratti^{a,b}, V. Re^a, M. Ressegotti^{a,b}, C. Riccardi^{a,b}, P. Salvini^a, I. Vai^{a,b}, P. Vitulo^{a,b}

INFN Sezione di Perugia ^a, Università di Perugia ^b, Perugia, Italy

L. Alunni Solestizi^{a,b}, M. Biasini^{a,b}, G.M. Bilei^a, C. Cecchi^{a,b}, D. Ciangottini^{a,b}, L. Fanò^{a,b}, P. Lariccia^{a,b}, R. Leonardi^{a,b}, E. Manoni^a, G. Mantovani^{a,b}, V. Mariani^{a,b}, M. Menichelli^a, A. Rossi^{a,b}, A. Santocchia^{a,b}, D. Spiga^a

INFN Sezione di Pisa ^a, Università di Pisa ^b, Scuola Normale Superiore di Pisa ^c, Pisa, Italy

K. Androsov^a, P. Azzurri^a, G. Bagliesi^a, L. Bianchini^a, T. Boccali^a, L. Borrello, R. Castaldi^a, M.A. Ciocci^{a,b}, R. Dell'Orso^a, G. Fedi^a, F. Fiori^{a,c}, L. Giannini^{a,c}, A. Giassi^a, M.T. Grippo^a, F. Ligabue^{a,c}, E. Manca^{a,c}, G. Mandorli^{a,c}, A. Messineo^{a,b}, F. Palla^a, A. Rizzi^{a,b}, P. Spagnolo^a, R. Tenchini^a, G. Tonelli^{a,b}, A. Venturi^a, P.G. Verdini^a

INFN Sezione di Roma ^a, Sapienza Università di Roma ^b, Rome, Italy

L. Barone^{a,b}, F. Cavallari^a, M. Cipriani^{a,b}, N. Daci^a, D. Del Re^{a,b}, E. Di Marco^{a,b}, M. Diemoz^a, S. Gelli^{a,b}, E. Longo^{a,b}, B. Marzocchi^{a,b}, P. Meridiani^a, G. Organtini^{a,b}, F. Pandolfi^a, R. Paramatti^{a,b}, F. Preiato^{a,b}, S. Rahatlou^{a,b}, C. Rovelli^a, F. Santanastasio^{a,b}

INFN Sezione di Torino ^a, Università di Torino ^b, Torino, Italy, Università del Piemonte Orientale ^c, Novara, Italy

N. Amapane^{a,b}, R. Arcidiacono^{a,c}, S. Argiro^{a,b}, M. Arneodo^{a,c}, N. Bartosik^a, R. Bellan^{a,b}, C. Biino^a, N. Cartiglia^a, F. Cenna^{a,b}, S. Cometti, M. Costa^{a,b}, R. Covarelli^{a,b}, N. Demaria^a, B. Kiani^{a,b}, C. Mariotti^a, S. Maselli^a, E. Migliore^{a,b}, V. Monaco^{a,b}, E. Monteil^{a,b}, M. Monteno^a, M.M. Obertino^{a,b}, L. Pacher^{a,b}, N. Pastrone^a, M. Pelliccioni^a, G.L. Pinna Angioni^{a,b}, A. Romero^{a,b}, M. Ruspa^{a,c}, R. Sacchi^{a,b}, K. Shchelina^{a,b}, V. Sola^a, A. Solano^{a,b}, D. Soldi, A. Staiano^a

INFN Sezione di Trieste ^a, Università di Trieste ^b, Trieste, Italy

S. Belforte^a, V. Candelise^{a,b}, M. Casarsa^a, F. Cossutti^a, G. Della Ricca^{a,b}, F. Vazzoler^{a,b}, A. Zanetti^a

Kyungpook National University

D.H. Kim, G.N. Kim, M.S. Kim, J. Lee, S. Lee, S.W. Lee, C.S. Moon, Y.D. Oh, S. Sekmen, D.C. Son, Y.C. Yang

Chonnam National University, Institute for Universe and Elementary Particles, Kwangju, Korea

H. Kim, D.H. Moon, G. Oh

Hanyang University, Seoul, Korea

J. Goh²⁹, T.J. Kim

Korea University, Seoul, Korea

S. Cho, S. Choi, Y. Go, D. Gyun, S. Ha, B. Hong, Y. Jo, K. Lee, K.S. Lee, S. Lee, J. Lim, S.K. Park, Y. Roh

Sejong University, Seoul, Korea

H.S. Kim

Seoul National University, Seoul, Korea

J. Almond, J. Kim, J.S. Kim, H. Lee, K. Lee, K. Nam, S.B. Oh, B.C. Radburn-Smith, S.h. Seo, U.K. Yang, H.D. Yoo, G.B. Yu

University of Seoul, Seoul, Korea

D. Jeon, H. Kim, J.H. Kim, J.S.H. Lee, I.C. Park

Sungkyunkwan University, Suwon, Korea

Y. Choi, C. Hwang, J. Lee, I. Yu

Vilnius University, Vilnius, Lithuania

V. Dudenas, A. Juodagalvis, J. Vaitkus

National Centre for Particle Physics, Universiti Malaya, Kuala Lumpur, Malaysia

I. Ahmed, Z.A. Ibrahim, M.A.B. Md Ali³⁰, F. Mohamad Idris³¹, W.A.T. Wan Abdullah, M.N. Yusli, Z. Zolkapli

Universidad de Sonora (UNISON), Hermosillo, Mexico

A. Castaneda Hernandez, J.A. Murillo Quijada

Centro de Investigacion y de Estudios Avanzados del IPN, Mexico City, Mexico

H. Castilla-Valdez, E. De La Cruz-Burelo, M.C. Duran-Osuna, I. Heredia-De La Cruz³², R. Lopez-Fernandez, J. Mejia Guisao, R.I. Rabadan-Trejo, M. Ramirez-Garcia, G. Ramirez-Sanchez, R Reyes-Almanza, A. Sanchez-Hernandez

Universidad Iberoamericana, Mexico City, Mexico

S. Carrillo Moreno, C. Oropeza Barrera, F. Vazquez Valencia

Benemerita Universidad Autonoma de Puebla, Puebla, Mexico

J. Eysermans, I. Pedraza, H.A. Salazar Ibarguen, C. Uribe Estrada

Universidad Autónoma de San Luis Potosí, San Luis Potosí, Mexico

A. Morelos Pineda

University of Auckland, Auckland, New Zealand

D. Krofcheck

University of Canterbury, Christchurch, New Zealand

S. Bheesette, P.H. Butler

National Centre for Physics, Quaid-I-Azam University, Islamabad, Pakistan

A. Ahmad, M. Ahmad, M.I. Asghar, Q. Hassan, H.R. Hoorani, A. Saddique, M.A. Shah, M. Shoaib, M. Waqas

National Centre for Nuclear Research, Swierk, Poland

H. Bialkowska, M. Bluj, B. Boimska, T. Frueboes, M. Górski, M. Kazana, K. Nawrocki, M. Szleper, P. Traczyk, P. Zalewski

Institute of Experimental Physics, Faculty of Physics, University of Warsaw, Warsaw, Poland

K. Bunkowski, A. Byzuk³³, K. Doroba, A. Kalinowski, M. Konecki, J. Krolikowski, M. Misiura, M. Olszewski, A. Pyskir, M. Walczak

Laboratório de Instrumentação e Física Experimental de Partículas, Lisboa, Portugal

M. Araujo, P. Bargassa, C. Beirão Da Cruz E Silva, A. Di Francesco, P. Faccioli, B. Galinhas, M. Gallinaro, J. Hollar, N. Leonardo, L. Lloret Iglesias, M.V. Nemallapudi, J. Seixas, G. Strong, O. Toldaiev, D. Vadrucio, J. Varela

Joint Institute for Nuclear Research, Dubna, Russia

S. Afanasiev, V. Alexakhin, P. Bunin, M. Gavrilenko, A. Golunov, I. Golutvin, N. Gorbounov, V. Karjavin, A. Lanev, A. Malakhov, V. Matveev^{34,35}, P. Moiseenz, V. Palichik, V. Perelygin, M. Savina, S. Shmatov, V. Smirnov, N. Voytishin, A. Zarubin

Petersburg Nuclear Physics Institute, Gatchina (St. Petersburg), Russia

V. Golovtsov, Y. Ivanov, V. Kim³⁶, E. Kuznetsova³⁷, P. Levchenko, V. Murzin, V. Oreshkin, I. Smirnov, D. Sosnov, V. Sulimov, L. Uvarov, S. Vavilov, A. Vorobyev

Institute for Nuclear Research, Moscow, Russia

Yu. Andreev, A. Dermenev, S. Gninenko, N. Golubev, A. Karneyeu, M. Kirsanov, N. Krasnikov, A. Pashenkov, D. Tlisov, A. Toropin

Institute for Theoretical and Experimental Physics, Moscow, Russia

V. Epshteyn, V. Gavrilov, N. Lychkovskaya, V. Popov, I. Pozdnyakov, G. Safronov, A. Spiridonov, A. Stepenov, V. Stolin, M. Toms, E. Vlasov, A. Zhokin

Moscow Institute of Physics and Technology, Moscow, Russia

T. Aushev

National Research Nuclear University 'Moscow Engineering Physics Institute' (MEPhI), Moscow, Russia

M. Chadeeva³⁸, P. Parygin, D. Philippov, S. Polikarpov³⁸, E. Popova, V. Rusinov

P.N. Lebedev Physical Institute, Moscow, Russia

V. Andreev, M. Azarkin³⁵, I. Dremin³⁵, M. Kirakosyan³⁵, S.V. Rusakov, A. Terkulov

Skobeltsyn Institute of Nuclear Physics, Lomonosov Moscow State University, Moscow, Russia

A. Baskakov, A. Belyaev, E. Boos, M. Dubinin³⁹, L. Dudko, A. Ershov, A. Gribushin, V. Klyukhin, O. Kodolova, I. Lokhtin, I. Miagkov, S. Obraztsov, S. Petrushanko, V. Savrin, A. Snigirev

Novosibirsk State University (NSU), Novosibirsk, Russia

V. Blinov⁴⁰, T. Dimova⁴⁰, L. Kardapoltsev⁴⁰, D. Shtol⁴⁰, Y. Skovpen⁴⁰

State Research Center of Russian Federation, Institute for High Energy Physics of NRC "Kurchatov Institute", Protvino, Russia

I. Azhgirey, I. Bayshev, S. Bitiukov, D. Elumakhov, A. Godizov, V. Kachanov, A. Kalinin, D. Konstantinov, P. Mandrik, V. Petrov, R. Ryutin, S. Slabospitskii, A. Sobol, S. Troshin, N. Tyurin, A. Uzunian, A. Volkov

National Research Tomsk Polytechnic University, Tomsk, Russia

A. Babaev, S. Baidali, V. Okhotnikov

University of Belgrade, Faculty of Physics and Vinca Institute of Nuclear Sciences, Belgrade, Serbia

P. Adzic⁴¹, P. Cirkovic, D. Devetak, M. Dordevic, J. Milosevic

Centro de Investigaciones Energéticas Medioambientales y Tecnológicas (CIEMAT), Madrid, Spain

J. Alcaraz Maestre, A. Álvarez Fernández, I. Bachiller, M. Barrio Luna, J.A. Brochero Cifuentes, M. Cerrada, N. Colino, B. De La Cruz, A. Delgado Peris, C. Fernandez Bedoya, J.P. Fernández Ramos, J. Flix, M.C. Fouz, O. Gonzalez Lopez, S. Goy Lopez, J.M. Hernandez, M.I. Josa, D. Moran, A. Pérez-Calero Yzquierdo, J. Puerta Pelayo, I. Redondo, L. Romero, M.S. Soares, A. Triossi

Universidad Autónoma de Madrid, Madrid, Spain

C. Albajar, J.F. de Trocóniz

Universidad de Oviedo, Oviedo, Spain

J. Cuevas, C. Erice, J. Fernandez Menendez, S. Folgueras, I. Gonzalez Caballero, J.R. González Fernández, E. Palencia Cortezon, V. Rodríguez Bouza, S. Sanchez Cruz, P. Vischia, J.M. Vizan Garcia

Instituto de Física de Cantabria (IFCA), CSIC-Universidad de Cantabria, Santander, Spain

I.J. Cabrillo, A. Calderon, B. Chazin Quero, J. Duarte Campderros, M. Fernandez, P.J. Fernández Manteca, A. García Alonso, J. Garcia-Ferrero, G. Gomez, A. Lopez Virto,

J. Marco, C. Martinez Rivero, P. Martinez Ruiz del Arbol, F. Matorras, J. Piedra Gomez, C. Prieels, T. Rodrigo, A. Ruiz-Jimeno, L. Scodellaro, N. Trevisani, I. Vila, R. Vilar Cortabitarte

CERN, European Organization for Nuclear Research, Geneva, Switzerland

D. Abbaneo, B. Akgun, E. Auffray, P. Baillon, A.H. Ball, D. Barney, J. Bendavid, M. Bianco, A. Bocci, C. Botta, E. Brondolin, T. Camporesi, M. Cepeda, G. Cerminara, E. Chapon, Y. Chen, G. Cucciati, D. d'Enterria, A. Dabrowski, V. Daponte, A. David, A. De Roeck, N. Deelen, M. Dobson, M. Dünser, N. Dupont, A. Elliott-Peisert, P. Everaerts, F. Fallavollita⁴², D. Fasanella, G. Franzoni, J. Fulcher, W. Funk, D. Gigi, A. Gilbert, K. Gill, F. Glege, M. Guilbaud, D. Gulhan, J. Hegeman, V. Innocente, A. Jafari, P. Janot, O. Karacheban¹⁸, J. Kieseler, A. Kornmayer, M. Krammer¹, C. Lange, P. Lecoq, C. Lourenço, L. Malgeri, M. Mannelli, F. Meijers, J.A. Merlin, S. Mersi, E. Meschi, P. Milenov⁴³, F. Moortgat, M. Mulders, J. Ngadiuba, S. Orfanelli, L. Orsini, F. Pantaleo¹⁵, L. Pape, E. Perez, M. Peruzzi, A. Petrilli, G. Petrucciani, A. Pfeiffer, M. Pierini, F.M. Pitters, D. Rabady, A. Racz, T. Reis, G. Rolandi⁴⁴, M. Rovere, H. Sakulin, C. Schäfer, C. Schwick, M. Seidel, M. Selvaggi, A. Sharma, P. Silva, P. Sphicas⁴⁵, A. Stakia, J. Steggemann, M. Tosi, D. Treille, A. Tsiros, V. Veckalns⁴⁶, W.D. Zeuner

Paul Scherrer Institut, Villigen, Switzerland

L. Caminada⁴⁷, K. Deiters, W. Erdmann, R. Horisberger, Q. Ingram, H.C. Kaestli, D. Kotlinski, U. Langenegger, T. Rohe, S.A. Wiederkehr

ETH Zurich - Institute for Particle Physics and Astrophysics (IPA), Zurich, Switzerland

M. Backhaus, L. Bäni, P. Berger, N. Chernyavskaya, G. Dissertori, M. Dittmar, M. Donegà, C. Dorfer, C. Grab, C. Heidegger, D. Hits, J. Hoss, T. Klijnsma, W. Luster, R.A. Manzoni, M. Marionneau, M.T. Meinhard, F. Micheli, P. Musella, F. Nessi-Tedaldi, J. Pata, F. Pauss, G. Perrin, L. Perrozzi, S. Pigazzini, M. Quittnat, D. Ruini, D.A. Sanz Becerra, M. Schönenberger, L. Shchutska, V.R. Tavolaro, K. Theofilatos, M.L. Vesterbacka Olsson, R. Wallny, D.H. Zhu

Universität Zürich, Zurich, Switzerland

T.K. Aarrestad, C. Amsler⁴⁸, D. Brzhechko, M.F. Canelli, A. De Cosa, R. Del Burgo, S. Donato, C. Galloni, T. Hreus, B. Kilminster, I. Neutelings, D. Pinna, G. Rauco, P. Robmann, D. Salerno, K. Schweiger, C. Seitz, Y. Takahashi, A. Zucchetta

National Central University, Chung-Li, Taiwan

Y.H. Chang, K.y. Cheng, T.H. Doan, Sh. Jain, R. Khurana, C.M. Kuo, W. Lin, A. Pozdnyakov, S.S. Yu

National Taiwan University (NTU), Taipei, Taiwan

P. Chang, Y. Chao, K.F. Chen, P.H. Chen, W.-S. Hou, Arun Kumar, Y.y. Li, Y.F. Liu, R.-S. Lu, E. Paganis, A. Psallidas, A. Steen

Chulalongkorn University, Faculty of Science, Department of Physics, Bangkok, Thailand

B. Asavapibhop, N. Srimanobhas, N. Suwonjandee

Çukurova University, Physics Department, Science and Art Faculty, Adana, Turkey

A. Bat, F. Boran, S. Cerci⁴⁹, S. Damarseckin, Z.S. Demiroglu, F. Dolek, C. Dozen, I. Dumanoglu, S. Girgis, G. Gokbulut, Y. Guler, E. Gurpinar, I. Hos⁵⁰, C. Isik, E.E. Kangal⁵¹, O. Kara, A. Kayis Topaksu, U. Kiminsu, M. Oglakci, G. Onengut, K. Ozdemir⁵², S. Ozturk⁵³, D. Sunar Cerci⁴⁹, B. Tali⁴⁹, U.G. Tok, S. Turkcapar, I.S. Zorbakir, C. Zorbilmez

Middle East Technical University, Physics Department, Ankara, Turkey

B. Isildak⁵⁴, G. Karapinar⁵⁵, M. Yalvac, M. Zeyrek

Bogazici University, Istanbul, Turkey

I.O. Atakisi, E. Gülmez, M. Kaya⁵⁶, O. Kaya⁵⁷, S. Tekten, E.A. Yetkin⁵⁸

Istanbul Technical University, Istanbul, Turkey

M.N. Agaras, S. Atay, A. Cakir, K. Cankocak, Y. Komurcu, S. Sen⁵⁹

Institute for Scintillation Materials of National Academy of Science of Ukraine, Kharkov, Ukraine

B. Grynyov

National Scientific Center, Kharkov Institute of Physics and Technology, Kharkov, Ukraine

L. Levchuk

University of Bristol, Bristol, United Kingdom

F. Ball, L. Beck, J.J. Brooke, D. Burns, E. Clement, D. Cussans, O. Davignon, H. Flacher, J. Goldstein, G.P. Heath, H.F. Heath, L. Kreczko, D.M. Newbold⁶⁰, S. Paramesvaran, B. Penning, T. Sakuma, D. Smith, V.J. Smith, J. Taylor, A. Titterton

Rutherford Appleton Laboratory, Didcot, United Kingdom

K.W. Bell, A. Belyaev⁶¹, C. Brew, R.M. Brown, D. Cieri, D.J.A. Cockerill, J.A. Coughlan, K. Harder, S. Harper, J. Linacre, E. Olaiya, D. Petyt, C.H. Shepherd-Themistocleous, A. Thea, I.R. Tomalin, T. Williams, W.J. Womersley

Imperial College, London, United Kingdom

G. Auzinger, R. Bainbridge, P. Bloch, J. Borg, S. Breeze, O. Buchmuller, A. Bundock, S. Casasso, D. Colling, L. Corpe, P. Dauncey, G. Davies, M. Della Negra, R. Di Maria, Y. Haddad, G. Hall, G. Iles, T. James, M. Komm, C. Laner, L. Lyons, A.-M. Magnan, S. Malik, A. Martelli, J. Nash⁶², A. Nikitenko⁷, V. Palladino, M. Pesaresi, A. Richards, A. Rose, E. Scott, C. Seez, A. Shtipliyski, G. Singh, M. Stoye, T. Strebler, S. Summers, A. Tapper, K. Uchida, T. Virdee¹⁵, N. Wardle, D. Winterbottom, J. Wright, S.C. Zenz

Brunel University, Uxbridge, United Kingdom

J.E. Cole, P.R. Hobson, A. Khan, P. Kyberd, C.K. Mackay, A. Morton, I.D. Reid, L. Teodorescu, S. Zahid

Baylor University, Waco, USA

K. Call, J. Dittmann, K. Hatakeyama, H. Liu, C. Madrid, B. McMaster, N. Pastika, C. Smith

Catholic University of America, Washington DC, USA

R. Bartek, A. Dominguez

The University of Alabama, Tuscaloosa, USA

A. Buccilli, S.I. Cooper, C. Henderson, P. Rumerio, C. West

Boston University, Boston, USA

D. Arcaro, T. Bose, D. Gastler, D. Rankin, C. Richardson, J. Rohlf, L. Sulak, D. Zou

Brown University, Providence, USA

G. Benelli, X. Coubez, D. Cutts, M. Hadley, J. Hakala, U. Heintz, J.M. Hogan⁶³, K.H.M. Kwok, E. Laird, G. Landsberg, J. Lee, Z. Mao, M. Narain, S. Piperov, S. Sagir⁶⁴, R. Syarif, E. Usai, D. Yu

University of California, Davis, Davis, USA

R. Band, C. Brainerd, R. Breedon, D. Burns, M. Calderon De La Barca Sanchez, M. Chertok, J. Conway, R. Conway, P.T. Cox, R. Erbacher, C. Flores, G. Funk, W. Ko, O. Kukral, R. Lander, C. Mclean, M. Mulhearn, D. Pellett, J. Pilot, S. Shalhout, M. Shi, D. Stolp, D. Taylor, K. Tos, M. Tripathi, Z. Wang, F. Zhang

University of California, Los Angeles, USA

M. Bachtis, C. Bravo, R. Cousins, A. Dasgupta, A. Florent, J. Hauser, M. Ignatenko, N. Mccoll, S. Regnard, D. Saltzberg, C. Schnaible, V. Valuev

University of California, Riverside, Riverside, USA

E. Bouvier, K. Burt, R. Clare, J.W. Gary, S.M.A. Ghiasi Shirazi, G. Hanson, G. Karapostoli, E. Kennedy, F. Lacroix, O.R. Long, M. Olmedo Negrete, M.I. Paneva, W. Si, L. Wang, H. Wei, S. Wimpenny, B.R. Yates

University of California, San Diego, La Jolla, USA

J.G. Branson, S. Cittolin, M. Derdzinski, R. Gerosa, D. Gilbert, B. Hashemi, A. Holzner, D. Klein, G. Kole, V. Krutelyov, J. Letts, M. Masciovecchio, D. Olivito, S. Padhi, M. Pieri, M. Sani, V. Sharma, S. Simon, M. Tadel, A. Vartak, S. Wasserbaech⁶⁵, J. Wood, F. Würthwein, A. Yagil, G. Zevi Della Porta

University of California, Santa Barbara - Department of Physics, Santa Barbara, USA

N. Amin, R. Bhandari, J. Bradmiller-Feld, C. Campagnari, M. Citron, A. Dishaw, V. Dutta, M. Franco Sevilla, L. Gouskos, R. Heller, J. Incandela, A. Ovcharova, H. Qu, J. Richman, D. Stuart, I. Suarez, S. Wang, J. Yoo

California Institute of Technology, Pasadena, USA

D. Anderson, A. Bornheim, J.M. Lawhorn, H.B. Newman, T.Q. Nguyen, M. Spiropulu, J.R. Vlimant, R. Wilkinson, S. Xie, Z. Zhang, R.Y. Zhu

Carnegie Mellon University, Pittsburgh, USA

M.B. Andrews, T. Ferguson, T. Mudholkar, M. Paulini, M. Sun, I. Vorobiev, M. Weinberg

University of Colorado Boulder, Boulder, USA

J.P. Cumalat, W.T. Ford, F. Jensen, A. Johnson, M. Krohn, S. Leontsinis, E. MacDonald, T. Mulholland, K. Stenson, K.A. Ulmer, S.R. Wagner

Cornell University, Ithaca, USA

J. Alexander, J. Chaves, Y. Cheng, J. Chu, A. Datta, K. Mcdermott, N. Mirman, J.R. Patterson, D. Quach, A. Rinkevicius, A. Ryd, L. Skinnari, L. Soffi, S.M. Tan, Z. Tao, J. Thom, J. Tucker, P. Wittich, M. Zientek

Fermi National Accelerator Laboratory, Batavia, USA

S. Abdullin, M. Albrow, M. Alyari, G. Apollinari, A. Apresyan, A. Apyan, S. Banerjee, L.A.T. Bauerdick, A. Beretvas, J. Berryhill, P.C. Bhat, G. Bolla[†], K. Burkett, J.N. Butler, A. Canepa, G.B. Cerati, H.W.K. Cheung, F. Chlebana, M. Cremonesi, J. Duarte, V.D. Elvira, J. Freeman, Z. Gecse, E. Gottschalk, L. Gray, D. Green, S. Grünendahl, O. Gutsche, J. Hanlon, R.M. Harris, S. Hasegawa, J. Hirschauer, Z. Hu, B. Jayatilaka, S. Jindariani, M. Johnson, U. Joshi, B. Klima, M.J. Kortelainen, B. Kreis, S. Lammel, D. Lincoln, R. Lipton, M. Liu, T. Liu, J. Lykken, K. Maeshima, J.M. Marraffino, D. Mason, P. McBride, P. Merkel, S. Mrenna, S. Nahn, V. O'Dell, K. Pedro, C. Pena, O. Prokofyev, G. Rakness, L. Ristori, A. Savoy-Navarro⁶⁶, B. Schneider, E. Sexton-Kennedy, A. Soha, W.J. Spalding, L. Spiegel, S. Stoynev, J. Strait, N. Strobbe, L. Taylor, S. Tkaczyk, N.V. Tran, L. Uplegger, E.W. Vaandering, C. Vernieri, M. Verzocchi, R. Vidal, M. Wang, H.A. Weber, A. Whitbeck

University of Florida, Gainesville, USA

D. Acosta, P. Avery, P. Bortignon, D. Bourilkov, A. Brinkerhoff, L. Cadamuro, A. Carnes, M. Carver, D. Curry, R.D. Field, S.V. Gleyzer, B.M. Joshi, J. Konigsberg, A. Korytov, P. Ma, K. Matchev, H. Mei, G. Mitselmakher, K. Shi, D. Sperka, J. Wang, S. Wang

Florida International University, Miami, USA

Y.R. Joshi, S. Linn

Florida State University, Tallahassee, USA

A. Ackert, T. Adams, A. Askew, S. Hagopian, V. Hagopian, K.F. Johnson, T. Kolberg, G. Martinez, T. Perry, H. Prosper, A. Saha, C. Schiber, V. Sharma, R. Yohay

Florida Institute of Technology, Melbourne, USA

M.M. Baarmand, V. Bhopatkar, S. Colafranceschi, M. Hohlmann, D. Noonan, M. Rahmani, T. Roy, F. Yumiceva

University of Illinois at Chicago (UIC), Chicago, USA

M.R. Adams, L. Apanasevich, D. Berry, R.R. Betts, R. Cavanaugh, X. Chen, S. Dittmer, O. Evdokimov, C.E. Gerber, D.A. Hangal, D.J. Hofman, K. Jung, J. Kamin, C. Mills, I.D. Sandoval Gonzalez, M.B. Tonjes, N. Varelas, H. Wang, X. Wang, Z. Wu, J. Zhang

The University of Iowa, Iowa City, USA

M. Alhusseini, B. Bilki⁶⁷, W. Clarida, K. Dilsiz⁶⁸, S. Durgut, R.P. Gandrajula, M. Haytmyradov, V. Khristenko, J.-P. Merlo, A. Mestvirishvili, A. Moeller, J. Nachtman, H. Ogul⁶⁹, Y. Onel, F. Ozok⁷⁰, A. Penzo, C. Snyder, E. Tiras, J. Wetzel

Johns Hopkins University, Baltimore, USA

B. Blumenfeld, A. Cocoros, N. Eminizer, D. Fehling, L. Feng, A.V. Gritsan, W.T. Hung, P. Maksimovic, J. Roskes, U. Sarica, M. Swartz, M. Xiao, C. You

The University of Kansas, Lawrence, USA

A. Al-bataineh, P. Baringer, A. Bean, S. Boren, J. Bowen, A. Bylinkin, J. Castle, S. Khalil, A. Kropivnitskaya, D. Majumder, W. Mcbrayer, M. Murray, C. Rogan, S. Sanders, E. Schmitz, J.D. Tapia Takaki, Q. Wang

Kansas State University, Manhattan, USA

S. Duric, A. Ivanov, K. Kaadze, D. Kim, Y. Maravin, D.R. Mendis, T. Mitchell, A. Modak, A. Mohammadi, L.K. Saini, N. Skhirtladze

Lawrence Livermore National Laboratory, Livermore, USA

F. Rebassoo, D. Wright

University of Maryland, College Park, USA

A. Baden, O. Baron, A. Belloni, S.C. Eno, Y. Feng, C. Ferraioli, N.J. Hadley, S. Jabeen, G.Y. Jeng, R.G. Kellogg, J. Kunkle, A.C. Mignerey, F. Ricci-Tam, Y.H. Shin, A. Skuja, S.C. Tonwar, K. Wong

Massachusetts Institute of Technology, Cambridge, USA

D. Abercrombie, B. Allen, V. Azzolini, A. Baty, G. Bauer, R. Bi, S. Brandt, W. Busza, I.A. Cali, M. D'Alfonso, Z. Demiragli, G. Gomez Ceballos, M. Goncharov, P. Harris, D. Hsu, M. Hu, Y. Iiyama, G.M. Innocenti, M. Klute, D. Kovalskyi, Y.-J. Lee, P.D. Luckey, B. Maier, A.C. Marini, C. Mcginn, C. Mironov, S. Narayanan, X. Niu, C. Paus, C. Roland, G. Roland, G.S.F. Stephans, K. Sumorok, K. Tatar, D. Velicanu, J. Wang, T.W. Wang, B. Wyslouch, S. Zhaozhong

University of Minnesota, Minneapolis, USA

A.C. Benvenuti, R.M. Chatterjee, A. Evans, P. Hansen, S. Kalafut, Y. Kubota, Z. Lesko, J. Mans, S. Nourbakhsh, N. Ruckstuhl, R. Rusack, J. Turkewitz, M.A. Wadud

University of Mississippi, Oxford, USA

J.G. Acosta, S. Oliveros

University of Nebraska-Lincoln, Lincoln, USA

E. Avdeeva, K. Bloom, D.R. Claes, C. Fangmeier, F. Golf, R. Gonzalez Suarez, R. Kamalieddin, I. Kravchenko, J. Monroy, J.E. Siado, G.R. Snow, B. Stieger

State University of New York at Buffalo, Buffalo, USA

A. Godshalk, C. Harrington, I. Iashvili, A. Kharchilava, D. Nguyen, A. Parker, S. Rappoccio, B. Roozbahani

Northeastern University, Boston, USA

G. Alverson, E. Barberis, C. Freer, A. Hortiangtham, D.M. Morse, T. Orimoto, R. Teixeira De Lima, T. Wamorkar, B. Wang, A. Wisecarver, D. Wood

Northwestern University, Evanston, USA

S. Bhattacharya, O. Charaf, K.A. Hahn, N. Mucia, N. Odell, M.H. Schmitt, K. Sung, M. Trovato, M. Velasco

University of Notre Dame, Notre Dame, USA

R. Bucci, N. Dev, M. Hildreth, K. Hurtado Anampa, C. Jessop, D.J. Karmgard, N. Kellams, K. Lannon, W. Li, N. Loukas, N. Marinelli, F. Meng, C. Mueller, Y. Musienko³⁴, M. Planer, A. Reinsvold, R. Ruchti, P. Siddireddy, G. Smith, S. Taroni, M. Wayne, A. Wightman, M. Wolf, A. Woodard

The Ohio State University, Columbus, USA

J. Alimena, L. Antonelli, B. Bylsma, L.S. Durkin, S. Flowers, B. Francis, A. Hart, C. Hill, W. Ji, T.Y. Ling, W. Luo, B.L. Winer, H.W. Wulsin

Princeton University, Princeton, USA

S. Cooperstein, P. Elmer, J. Hardenbrook, S. Higginbotham, A. Kalogeropoulos, D. Lange, M.T. Lucchini, J. Luo, D. Marlow, K. Mei, I. Ojalvo, J. Olsen, C. Palmer, P. Piroué, J. Salfeld-Nebgen, D. Stickland, C. Tully

University of Puerto Rico, Mayaguez, USA

S. Malik, S. Norberg

Purdue University, West Lafayette, USA

A. Barker, V.E. Barnes, S. Das, L. Gutay, M. Jones, A.W. Jung, A. Khatiwada, B. Mahakud, D.H. Miller, N. Neumeister, C.C. Peng, H. Qiu, J.F. Schulte, J. Sun, F. Wang, R. Xiao, W. Xie

Purdue University Northwest, Hammond, USA

T. Cheng, J. Dolen, N. Parashar

Rice University, Houston, USA

Z. Chen, K.M. Ecklund, S. Freed, F.J.M. Geurts, M. Kilpatrick, W. Li, B. Michlin, B.P. Padley, J. Roberts, J. Rorie, W. Shi, Z. Tu, J. Zabel, A. Zhang

University of Rochester, Rochester, USA

A. Bodek, P. de Barbaro, R. Demina, Y.t. Duh, J.L. Dulemba, C. Fallon, T. Ferbel, M. Galanti, A. Garcia-Bellido, J. Han, O. Hindrichs, A. Khukhunaishvili, K.H. Lo, P. Tan, R. Taus, M. Verzetti

Rutgers, The State University of New Jersey, Piscataway, USA

A. Agapitos, J.P. Chou, Y. Gershtein, T.A. Gómez Espinosa, E. Halkiadakis, M. Heindl, E. Hughes, S. Kaplan, R. Kunnawalkam Elayavalli, S. Kyriacou, A. Lath, R. Montalvo, K. Nash, M. Osherson, H. Saka, S. Salur, S. Schnetzer, D. Sheffield, S. Somalwar, R. Stone, S. Thomas, P. Thomassen, M. Walker

University of Tennessee, Knoxville, USA

A.G. Delannoy, J. Heideman, G. Riley, S. Spanier, K. Thapa

Texas A&M University, College Station, USA

O. Bouhali⁷¹, A. Celik, M. Dalchenko, M. De Mattia, A. Delgado, S. Dildick, R. Eusebi, J. Gilmore, T. Huang, T. Kamon⁷², S. Luo, R. Mueller, R. Patel, A. Perloff, L. Perniè, D. Rathjens, A. Safonov

Texas Tech University, Lubbock, USA

N. Akchurin, J. Damgov, F. De Guio, P.R. Duderov, S. Kunori, K. Lamichhane, S.W. Lee, T. Mengke, S. Muthumuni, T. Peltola, S. Undleeb, I. Volobouev, Z. Wang

Vanderbilt University, Nashville, USA

S. Greene, A. Gurrola, R. Janjam, W. Johns, C. Maguire, A. Melo, H. Ni, K. Padeken, J.D. Ruiz Alvarez, P. Sheldon, S. Tuo, J. Velkovska, M. Verweij, Q. Xu

University of Virginia, Charlottesville, USA

M.W. Arenton, P. Barria, B. Cox, R. Hirosky, M. Joyce, A. Ledovskoy, H. Li, C. Neu, T. Sinthuprasith, Y. Wang, E. Wolfe, F. Xia

Wayne State University, Detroit, USA

R. Harr, P.E. Karchin, N. Poudyal, J. Sturdy, P. Thapa, S. Zaleski

University of Wisconsin - Madison, Madison, WI, USA

M. Brodski, J. Buchanan, C. Caillol, D. Carlsmith, S. Dasu, L. Dodd, B. Gomber, M. Grothe, M. Herndon, A. Hervé, U. Hussain, P. Klabbers, A. Lanaro, A. Levine, K. Long, R. Loveless, T. Ruggles, A. Savin, N. Smith, W.H. Smith, N. Woods

†: Deceased

1: Also at Vienna University of Technology, Vienna, Austria

2: Also at IRFU, CEA, Université Paris-Saclay, Gif-sur-Yvette, France

3: Also at Universidade Estadual de Campinas, Campinas, Brazil

4: Also at Federal University of Rio Grande do Sul, Porto Alegre, Brazil

5: Also at Université Libre de Bruxelles, Bruxelles, Belgium

6: Also at University of Chinese Academy of Sciences, Beijing, China

7: Also at Institute for Theoretical and Experimental Physics, Moscow, Russia

8: Also at Joint Institute for Nuclear Research, Dubna, Russia

9: Also at Cairo University, Cairo, Egypt

10: Also at Helwan University, Cairo, Egypt

11: Now at Zewail City of Science and Technology, Zewail, Egypt

12: Also at Department of Physics, King Abdulaziz University, Jeddah, Saudi Arabia

13: Also at Université de Haute Alsace, Mulhouse, France

14: Also at Skobeltsyn Institute of Nuclear Physics, Lomonosov Moscow State University, Moscow, Russia

15: Also at CERN, European Organization for Nuclear Research, Geneva, Switzerland

16: Also at RWTH Aachen University, III. Physikalisches Institut A, Aachen, Germany

17: Also at University of Hamburg, Hamburg, Germany

18: Also at Brandenburg University of Technology, Cottbus, Germany

19: Also at MTA-ELTE Lendület CMS Particle and Nuclear Physics Group, Eötvös Loránd University, Budapest, Hungary

20: Also at Institute of Nuclear Research ATOMKI, Debrecen, Hungary

21: Also at Institute of Physics, University of Debrecen, Debrecen, Hungary

22: Also at Indian Institute of Technology Bhubaneswar, Bhubaneswar, India

- 23: Also at Institute of Physics, Bhubaneswar, India
- 24: Also at Shoolini University, Solan, India
- 25: Also at University of Visva-Bharati, Santiniketan, India
- 26: Also at Isfahan University of Technology, Isfahan, Iran
- 27: Also at Plasma Physics Research Center, Science and Research Branch, Islamic Azad University, Tehran, Iran
- 28: Also at Università degli Studi di Siena, Siena, Italy
- 29: Also at Kyunghee University, Seoul, Korea
- 30: Also at International Islamic University of Malaysia, Kuala Lumpur, Malaysia
- 31: Also at Malaysian Nuclear Agency, MOSTI, Kajang, Malaysia
- 32: Also at Consejo Nacional de Ciencia y Tecnología, Mexico city, Mexico
- 33: Also at Warsaw University of Technology, Institute of Electronic Systems, Warsaw, Poland
- 34: Also at Institute for Nuclear Research, Moscow, Russia
- 35: Now at National Research Nuclear University 'Moscow Engineering Physics Institute' (MEPhI), Moscow, Russia
- 36: Also at St. Petersburg State Polytechnical University, St. Petersburg, Russia
- 37: Also at University of Florida, Gainesville, USA
- 38: Also at P.N. Lebedev Physical Institute, Moscow, Russia
- 39: Also at California Institute of Technology, Pasadena, USA
- 40: Also at Budker Institute of Nuclear Physics, Novosibirsk, Russia
- 41: Also at Faculty of Physics, University of Belgrade, Belgrade, Serbia
- 42: Also at INFN Sezione di Pavia ^a, Università di Pavia ^b, Pavia, Italy
- 43: Also at University of Belgrade, Faculty of Physics and Vinca Institute of Nuclear Sciences, Belgrade, Serbia
- 44: Also at Scuola Normale e Sezione dell'INFN, Pisa, Italy
- 45: Also at National and Kapodistrian University of Athens, Athens, Greece
- 46: Also at Riga Technical University, Riga, Latvia
- 47: Also at Universität Zürich, Zurich, Switzerland
- 48: Also at Stefan Meyer Institute for Subatomic Physics (SMI), Vienna, Austria
- 49: Also at Adiyaman University, Adiyaman, Turkey
- 50: Also at Istanbul Aydin University, Istanbul, Turkey
- 51: Also at Mersin University, Mersin, Turkey
- 52: Also at Piri Reis University, Istanbul, Turkey
- 53: Also at Gaziosmanpasa University, Tokat, Turkey
- 54: Also at Ozyegin University, Istanbul, Turkey
- 55: Also at Izmir Institute of Technology, Izmir, Turkey
- 56: Also at Marmara University, Istanbul, Turkey
- 57: Also at Kafkas University, Kars, Turkey
- 58: Also at Istanbul Bilgi University, Istanbul, Turkey
- 59: Also at Hacettepe University, Ankara, Turkey
- 60: Also at Rutherford Appleton Laboratory, Didcot, United Kingdom
- 61: Also at School of Physics and Astronomy, University of Southampton, Southampton, United Kingdom
- 62: Also at Monash University, Faculty of Science, Clayton, Australia
- 63: Also at Bethel University, St. Paul, USA
- 64: Also at Karamanoğlu Mehmetbey University, Karaman, Turkey
- 65: Also at Utah Valley University, Orem, USA
- 66: Also at Purdue University, West Lafayette, USA
- 67: Also at Beykent University, Istanbul, Turkey

68: Also at Bingol University, Bingol, Turkey

69: Also at Sinop University, Sinop, Turkey

70: Also at Mimar Sinan University, Istanbul, Istanbul, Turkey

71: Also at Texas A&M University at Qatar, Doha, Qatar

72: Also at Kyungpook National University, Daegu, Korea